IEEE Access
Multidisciplinary ⋮ Rapid Review ⋮ Open Access Journal

Received 10 July 2023, accepted 29 July 2023, date of publication 2 August 2023, date of current version 9 August 2023.

Digital Object Identifier 10.1109/ACCESS.2023.3301181

RESEARCH ARTICLE

Asymmetric System Model Parameters Identification Framework via Relay Feedback

LIBOR PEKAŘ[1,2], (Member, IEEE), RADEK MATUŠŮ[3], (Member, IEEE), MENGJIE SONG[4], LENKA KUKLIŠOVÁ PAVELKOVÁ[2,5], AND QINGBIN GAO[6]

[1]Department of Automation and Control Engineering, Faculty of Applied Informatics, Tomas Bata University in Zlín, 76001 Zlín, Czech Republic
[2]Department of Technical Studies, College of Polytechnics Jihlava, 58601 Jihlava, Czech Republic
[3]Faculty of Applied Informatics, Centre for Security, Information and Advanced Technologies (CEBIA–Tech), Tomas Bata University in Zlín, 76001 Zlín, Czech Republic
[4]Department of Energy and Power Engineering, School of Mechanical Engineering, Beijing Institute of Technology, Haidian, Beijing 100081, China
[5]Institute of Information Theory and Automation, Czech Academy of Sciences, 18200 Prague, Czech Republic
[6]School of Mechanical Engineering and Automation, Harbin Institute of Technology, Nanshan, Shenzhen 518055, China

Corresponding author: Libor Pekař (pekar@utb.cz)

This work was supported in part by the College of Polytechnics Jihlava, under Grant INT/2022/0002 ''Identification and Control of Time-Delay Systems via Parameter Optimization Methods'', in part by the Czech Science Foundation under Grant GAČR 21-45465L, and in part by the National Foreign Expert Project under Grant G2022178023L.

ABSTRACT This paper proposes an innovative framework of a parameter estimation procedure based on the well-established relay-feedback experiment paradigm. The novelty consists in consideration of asymmetric dynamics and non-equal static gains of the identified system. A different system behavior after changing the input variable polarity near the operating point is rarely considered or even omitted within relay-based parameter identification tests, in contrast to the common use of asymmetry in the nonlinear relay element. The thing is that many existing relay-based identification techniques in the frequency domain use integrations, assuming that the system output operating point coincides with the setpoint value (i.e., the offset between them is zero). However, this is not true for asymmetric dynamic systems, which yields considerably erroneous parameter estimation as the integration result is highly sensitive to the baseline value. The resulting iterative numerical optimization-based algorithm is built-up using a chain of natural assumptions and step-by-step thought experiments. The proposed framework is applied to the well-established exponential decaying method in this paper. Some computation aspects of the algorithm are discussed. A comparative numerical study illustrates the efficacy of the proposed strategy, where several frequency-fitting-based and descriptive-function-based competitive approaches are considered.

INDEX TERMS Asymmetric dynamics, frequency-domain analysis, optimization, parameter estimation, relay feedback, system dynamics, system identification.

I. INTRODUCTION

When modeling and identifying parameters of dynamic systems, it is usually assumed that the system dynamics and the static gain remain invariant with respect to the input polarity in the neighborhood of the operating point. It implies that a unique model is considered regardless of the relative change of the input variable sign. However, static and dynamic system behavior can differ for a positive and a negative input variable change. Regarding static gain values, this fact is obvious from the static characteristics of nonlinear systems, see Fig. 1 (and the description therein). Naturally, static gains (as the tangents to the characteristics) are non-equal in the left and right operating point neighborhoods. Besides, scholars have referred to many systems and processes with asymmetric dynamics appearing in various scientific and engineering fields, ranging from microcosmos to complex atmospheric phenomena modeling. To name just a few, Zhang et al. [1] showed generic asymmetric expansion and correlation dynamics in non-Hermitian quantum many-body systems. Zushi and Takeuchi [2] studied spontaneous symmetry restoring for asymmetric dynamics of liquid-crystal

The associate editor coordinating the review of this manuscript and approving it for publication was Sotirios Goudos.

reconnecting disclinations. Han et al. [3] proposed an extended Rayleigh-Plesset model to predict the asymmetric dynamics of a cavitation bubble. In [4], a DC-offset-induced asymmetric dynamical behavior in Memristive Chua's circuits was revealed using equilibrium point analyses, numerical simulations, and experimental measurements. Asymmetric dynamics can inherently be detected in heat and mass transfer systems and processes. For instance, Vasičkaninová et al. [5] referred to an asymmetric dynamics of a heat-exchanger network when fuzzy-logic control designing. Rodriguez and Campo [6] showed that the vortex shedding process in a forced convection heat transfer is asymmetric for high values of Reynolds number and low values of Prandtl numbers. Kim et al. [7] observed a strong spatiotemporal asymmetry between the inflow and outflow from the downstream and the upstream, respectively, during the power generation phase in a tidal power plant. Asymmetric dynamics models are not limited to technical and engineering problems. The asymmetric mean-reverting fundamental dynamics governing the unemployment rate based on a simple labor supply and demand relationship model was derived in [8]. Simonyan and Bayraktar [9] studied asymmetric relationships between sovereign credit default swaps and variables in bull and bear markets. Last but not least, asymmetric systems can also be found in wild nature. For instance, Cheng et al. [10] referred to the existence of asymmetric processes in the typhoon secondary eyewall formation mechanism.

The relay-feedback experiment has become one of the most favorite and widely used parameter identification principles in practice [11], [12]. Its nascence can be traced back to the early 1950s [13]; however, the work by Aström and Hägglund [14] is usually considered as the pioneering result in the field. This parameter-identification task is usually followed by automatic controller tuning, which represents the autotuning procedure [14], [15]. Main advantages of this concept can be summarized as follows: It can even be applied to integral or unstable processes that are stabilizable by the feedback loop with a relay, and, in particular, the process output is kept close to the setpoint, which is favorable or even required in various industrial applications.

The main idea lies in the existence of sustained oscillations that enable estimating the ultimate (or other) frequency points of the model by detecting process output shape, angular frequency, phase shift, and amplitude.

Two frequency-based families and a time-domain one of relay-feedback data evaluation for the model parameter identification can be found in the literature [11]. The so-called describing function (DF) represents the most used frequency-domain method that utilizes harmonic analysis and linear approximation of the relay output [16], [17].

The original concept [14] used a simple symmetric on/off relay; however, it was shown that the obtained ultimate gains could have errors of over 15% [18]. Therefore, scholars investigated different techniques to enhance the DF and ultimate-frequency point estimation.

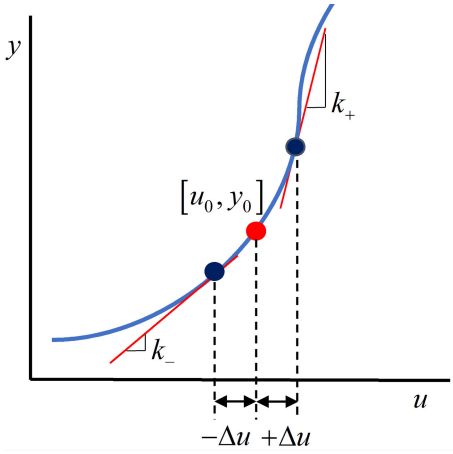

FIGURE 1. The static characteristics of a nonlinear system where u is the input and y means the output. If a negative change $-\Delta u$ of the input value in the neighborhood of the operating point $[u_0, y_0]$ is made, the corresponding static gain k^- differs from that (k^+) under a positive input change $+\Delta u$.

For instance, a relay with hysteresis [19], [20], a saturated relay [21], a parasitic or a cascade relay [22], preload relay [23], or a multiple-switching relay [24] were used to cope with this task. Ghorai et al. [25] developed an online technique that includes a proportionally-derivative controller within the identification procedure. Other methods, e.g., use asymmetric sustained oscillations [26] or attempt to reduce disturbances and noises [27], [28].

The fitting of the frequency-response points represents another bunch of methods [29], [30], [31]. Whereas the DF methods attempt to match the ultimate-frequency point or a low number of other points, the frequency fitting (FF) approaches aim to match a multitude of frequency points. The fact is that the simple test can estimate only one point giving rise to two model parameter values. Various strategies were proposed to estimate more points (generally, extract more information from the closed-loop responses). For instance, an artificial integrator or a delay element can be inserted in the open loop to reach a preset phase shift [32], [33]. Hofreiter [34] proposed a 2-shifting method that enables estimating two frequency-response points. This idea has been extended to several n-shifting methods [32], [35]. The FF approaches also utilize modified integrable relay inputs and outputs by reducing the magnitudes via exponential decay [36] or a shifting procedure [18]. Miguel-Escrig et al. [12] recently designed a complex method based on algebraic operations and a proper selection of frequency-response points that were estimated corresponding to the fundamental oscillation frequency induced by the asymmetric relay and its harmonics.

Time-domain methods usually aim to match the course of the identified system output caused by the relay feedback with the model theoretical response using its analytic

formulation [37], [38]. Kyeong et. al. [39] proposed a technique combining DF and time-domain approaches that is insensitive to static disturbances.

The main motivation for this research has arisen from the following observation. It is intrinsically considered that the system output operating point equals the setpoint value for the closed relay-feedback loop (i.e., the offset between them is zero). This natural assumption, however, holds for systems and processes with ideally symmetric static gain and model dynamics parameters. It was observed that the output operating point differs from the setpoint if an identified system asymmetry appears. Note that the rationale behind this effect is provided in Section III. Moreover, the same rationale implies that not only one but two shifts must exist – for the positive input change and the negative one. It gives rise to two different subsystems with non-equal dynamics and static parameters.

Whereas the accuracy of DF-based methods usually does not depend on either the reference value or the operating point value [39] (but only the difference between response extrema is evaluated), the FF relay-feedback identification methods yield erroneous parameter estimation if there is a mismatch between the reference value and the output operating point. This fact is because of integral computations for the parameters' evaluation, the accuracy of which is highly sensitive to the zero-point guess (see Sections II and III). Theoretically, if the exact offset value is found, the static gain and other dynamic parameters can be analytically determined [11], [36]. Hence, it is crucial to estimate operating points for each subsystem as accurately as possible by available numerical means.

According to the authors' best knowledge, no method that proposes estimating the offset value for asymmetric systems exists. In contrast to the use of the asymmetric relay for standard symmetric processes [12], [26], [28], [32], [36], the effect of an asymmetric relay on systems with asymmetric response has not been considered yet. However, several methods have been investigated for tackling a process output shift due to disturbance when performing relay-based parameter identification. These techniques attempt to restore symmetry by various means (e.g., by an adaptive setting of the relay asymmetry [28], high-pass filtering [40], moving the reference value [41], etc.). Although they can overcome the signal asymmetry (regardless of the reason), they do not consider the offset change.

The presented research represents the framework strategy for a family of FF techniques for asymmetric identified systems. Its contribution can be summarized as follows:

1) The exact output mean value for symmetric identified systems when using an asymmetric (biased) relay is derived. Based on this value, an initial static-gain guess can be made for asymmetric systems.
2) The iterative estimation formula for computing the system output operating point is derived using the preceding results.
3) The iteratively updated operating point value yields the direct reset of the static gain guess, and model parameters are successively estimated by solving a nonlinear optimization problem based on the multiple-point decay-based identification method [36].
4) The efficacy of the proposed relay-based strategy is illustrated via a comparative academic example. The relay with hysteresis [19], the saturation relay [21], and an output drift compensation followed by asymmetric input excitation serve as competitive DF-based methods [40]. An n-shifting procedure with artificial delay [32] and a full closed-loop test with a special activation function [18] are representatives of FF-based methods. In addition, the reasonability of the proposed method is demonstrated by showing identification results when the offset is zero (i.e., the reference value is assumed to be equal to the output operating point).

The remainder of this paper is organized as follows. Section II introduces preliminaries of the framework idea of the relay-feedback identification test using DFs and describes the multiple-point FF-based method with signal decaying. The motivation and the research problem in question are raised in Section III. The main result crowned by the iterative identification procedure for asymmetric systems is provided in Section IV. In Section V, a numerical academic example demonstrating the proposed strategy is given. Some computational aspects of the algorithm are discussed, and a comparative study is elaborated along with a concise description of the competitive methods. Conclusions are drawn in Section VI.

II. PRELIMINARIES

The basic general principle of the relay-feedback parameter identification test is introduced in this section. The idea of using DF and FF-based methods for the relay-based identification, and the exponential decay method [36] are concisely summarized as well. Note that advanced techniques are omitted due to brevity; interested readers are referred to, e.g., [11], [12], and [22] for more details. Particular comparative methods benchmarked in this research are introduced in Section V.

The relay-feedback scheme is depicted in Fig. 2 where "Plant" expresses the identified system, "Relay" means the nonlinear relay element, "Add" stands for a potential additional artificial linear dynamics (see, e.g., [25], [32], [33]), reference (setpoint), error, system input, and output variables are denoted by $r(t)$, $e(t)$, $u(t)$, and $y(t)$, respectively (note that the time argument (t) is omitted in the figure). Under some conditions, sustained oscillations with angular frequency $\omega_{osc} = 2\pi/T_{os}$ appear after time t_{os}.

A. RELAY-FEEDBACK IDENTIFICATION FRAMEWORK

The idea of using a DF $N_{DF}(\cdot) \in C$ for model parameter identification stems from a linear approximation of the relay dynamics, giving rise to the estimation of a single point of the model frequency response (1).

$$G_m(\mathrm{j}\omega_{os}) = -\frac{1}{G_a(\mathrm{j}\omega_{os})\, N_{DF}(\cdot)} \tag{1}$$

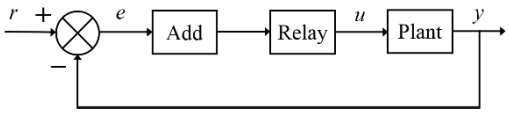

FIGURE 2. A general scheme of the parameter identification principle via a relay in the feedback.

Equivalently, one can write

$$\begin{cases} |G_m(\mathrm{j}\omega_{os})| = \dfrac{1}{|G_a(\mathrm{j}\omega_{os})\, N_{DF}(\cdot)|}, \\ G_m(\mathrm{j}\omega_{os}) = -\left[G_a(\mathrm{j}\omega_{os}) + N_{DF}(\cdot) + \pi\right] \end{cases} \tag{2}$$

where $G_m(s)$, $G_a(s)$ are the plant model and the additional element transfer functions, respectively, and $\mathrm{j}^2 = -1$. The formulae express that the overall open-loop gain is -1 and the phase shift equals $-\pi$. The DF $N_{DF}(\cdot)$ depends on various relay parameters and the output sustained oscillation amplitude $A = 0.5\,[y(t_{\max}) - y(t_{\min})]$ where $t_{\max} = \arg\max_{t \geq t_{os}} y(t)$, $t_{\min} = \arg\min_{t \geq t_{os}} y(t)$

The core of most FF-based methods lies in Lemma 1 [18], [32], [42].

Lemma 1 (Laplace Transform of Periodic Function): Let $f : [0, \infty) \to R$ be a periodic function of period $T_{os} > 0$ (i.e., $f(t) = f(t + T_{os})$ for all $t \geq 0$). If the Laplace transform of f exist, then

$$F(s) = L\{f(t)\} = \frac{\int_0^{T_{os}} f(t) \exp(-st)\,\mathrm{d}t}{1 - \exp(-sT_{os})} \tag{3}$$

Lemma 1 implies that the model transfer function can be written as

$$G_m(s) = \frac{L\{y(t)\}}{L\{u(t)\}} = \frac{Y(s)}{U(s)} = \frac{\int_t^{t+T_{os}} y(t) \exp(-st)\,\mathrm{d}t}{\int_t^{t+T_{os}} u(t) \exp(-st)\,\mathrm{d}t} \tag{4}$$

for $t \geq t_{os}$. The corresponding frequency response can be obtained by substituting $\mathrm{j}\omega \leftarrow s$

$$G_m(\mathrm{j}\omega) = \frac{\int_t^{t+T_{os}} y(t) \exp(-\mathrm{j}\omega t)\,\mathrm{d}t}{\int_t^{t+T_{os}} u(t) \exp(-\mathrm{j}\omega t)\,\mathrm{d}t} \tag{5}$$

Although in literature, formula (5) is assumed to be applied for $\omega = 0$ or $\omega = \omega_{os}$ only, it can also be used for other frequencies. The former yields the model static gain guess

$$k = G_m(0) = \frac{\int_t^{t+T_{os}} y(t)\,\mathrm{d}t}{\int_t^{t+T_{os}} u(t)\,\mathrm{d}t} \tag{6}$$

B. EXPONENTIAL DECAY METHOD

Let us introduce a well-established FF method used in this research. Namely, the exponential decay method [36] enables estimating multiple frequency points under a single relay test.

First, process input and output are subject to the decaying

$$\begin{aligned} u_a(t) &= u(t) \exp(-at), \\ y_a(t) &= y(t) \exp(-at), \\ a &> 0, \quad t \in [0, t_f] \end{aligned} \tag{7}$$

where t_f expresses the relay experiment duration, for which $|u_a(t)|, |y_a(t)|$ within $t \in (t_f - T_{os}, t_f] := I_f$ are sufficiently small. The decaying satisfies the integrability of the signals. Clearly, if $\varepsilon_a > \max(|u_a(t)|, |y_a(t)|)$, $t \in I_f$, is selected, the decaying exponent a must be taken as

$$a > \frac{1}{t} \ln\left[\frac{\max(|u(t)|, |y(t)|)}{\varepsilon_a}\right], \; t \in I_f \tag{8}$$

According to [43], a suitable option is $\varepsilon_a \approx (10^{-6} \sim 10^{-4}) \max(|u(t)|, |y(t)|)$. In [18], it is suggested to take $a = 0.05\omega_{os}$.

Then, the shifted model Laplace transform reads

$$\begin{aligned} G_m(s + a) &= \frac{L\{y_a(t)\}}{L\{u_a(t)\}} \\ &= \frac{Y(s + a)}{U(s + a)} = \frac{\int_0^{t_f} y_a(t) \exp(-st)\,\mathrm{d}t}{\int_0^{t_f} u_a(t) \exp(-st)\,\mathrm{d}t} \end{aligned} \tag{9}$$

By substituting $\mathrm{j}\omega \leftarrow s$ and setting $\omega = \omega_l \geq 0$, $l = 0, 1, \ldots$, the following set of algebraic equations is obtained

$$G_m(\mathrm{j}\omega_l + a) = \frac{\int_0^{t_f} y_a(t) \exp(-\mathrm{j}\omega_l t)\,\mathrm{d}t}{\int_0^{t_f} u_a(t) \exp(-\mathrm{j}\omega_l t)\,\mathrm{d}t} \tag{10}$$

where the left-hand side of (10) includes unknown model parameter values, whereas the right-hand one is computed from the relay-test data. In practice, measured signals are sampled with the period T_s, and the discrete-time Fourier transform (DTFT) is used to compute (10)

$$G_m(\mathrm{j}\omega_l + a) \approx \frac{\sum_{i=0}^{N-1} y_a(t_i) \exp(-\mathrm{j}\omega_l t_i)}{\sum_{i=0}^{N-1} u_a(t_i) \exp(-\mathrm{j}\omega_l t_i)} \tag{11}$$

where $t_{i+1} = t_i + T_s$ and N means the number of samples. The original work [36], [43] suggests taking

$$\omega_l = l\frac{2\pi}{NT_s}, \; l = \overline{0, M-1}; \; M \leq N\frac{T_s}{T_{os}} + 1 \tag{12}$$

where M is the number of considered frequency points. In fact, $u(t)$, $y(t)$ represents the deviation from the operating point $[u_0, y_0]$ in academic formulae (4)-(7). Hence, the following differences should be substituted in the formulae instead of $u(t)$, $y(t)$:

$$\Delta u(t) = u(t) - u_0, \; \Delta y(t) = y(t) - y_0 \tag{13}$$

Besides, formula (10) holds for any $\omega_l \in R$; hence, the simple quadrature (11) can consider different angular frequencies than those in (12). Note that the corresponding quadrature can be applied to (5).

III. RESEARCH PROBLEM

This section provides the reader with research problem motivation and formulation. The problem arises from the existence of identified process asymmetry that cannot be a priori excluded.

A. MOTIVATION

The accuracy of FF methods strongly depends on integral values (5), (6), or (10). These formulae include input and output differences (13) that are functions of the operating point $[u_0, y_0]$. Clearly, if an integrand is shifted by d in a particular integral with lower and upper limits L_1 and L_2, respectively, then the integral error is $d\,(L_2 - L_1)$.

However, systems with asymmetric dynamics and/or static gain reveal a mismatch between the reference value r and the output operating point value y_0. Then the obtained results are considerably erroneous when computing integrals around the setpoint. We have observed the described effect when performing standard relay-based identification experiments in a laboratory [44]. To judge this effect rigorously, it is possible to formulate the following simple lemma.

Lemma 2: Given an asymmetric identified system in the relay-feedback loop, a unique output operating value $y_0 = r$ does not exist.

Proof: Let $G_+(s)$ and $G_-(s)$ express different asymmetric subsystems' dynamics for positive ($\Delta u > 0$) and negative ($\Delta u < 0$) input step changes, respectively, due to the relay switching. Consider a contradiction: Let the unique $y_0 = r$ exist for both subsystems. Then (5) (or (10)) and (6) return identical dynamic and static, respectively, frequency responses $G_m(\cdot)$ for both subsystems. It means that $G_+(s) = G_-(s)$, which yields a contradiction. ■

Hence, two research questions arise:

RQ1: How can the real (true) value of y_0 for each submodel be estimated?

RQ2: How can unknown parameters of particular models $G_{m+}(s)$ and $G_{m-}(s)$ be estimated?

The formulation of these problems in detail follows.

B. PROBLEM FORMULATION

Consider a biased (asymmetric output) relay with a symmetric (input) hysteresis, for simplicity, switching as follows

$$u(t) = \begin{cases} B_+ = u_0 + B + \delta, \\ \quad \text{if} \quad (e(t) \geq \varepsilon) \vee (-\varepsilon \leq e(t) \leq \varepsilon \wedge \dot{e}(t) < 0) \\ B_- = u_0 - B + \delta, \\ \quad \text{if} \quad (e(t) \leq -\varepsilon) \vee (-\varepsilon \leq e(t) \leq \varepsilon \wedge \dot{e}(t) > 0) \end{cases} \tag{14}$$

where $B = 0.5\,(B_+ - B_-)$ and $\delta \neq 0$ expresses the relay asymmetry (bias). Note that hysteresis $\varepsilon \geq 0$ helps to overcome excessive switching rates under signal disturbances in practice. The corresponding static characteristics is depicted in Fig. 3 and its DF reads [35]

$$N_{DF}(A, B, \Delta A, \varepsilon) = \frac{2B}{\pi A}\left[\sqrt{1 - \left(\frac{-\Delta A - \varepsilon}{A}\right)^2} + \sqrt{1 - \left(\frac{-\Delta A + \varepsilon}{A}\right)^2}\right] + \frac{4B\varepsilon}{\pi A^2}\mathrm{j} \tag{15}$$

where $A = 0.5\,(y_{\max} - y_{\min})$ is the amplitude of the sustained oscillations and $\Delta A := 0.5\,(y_{\max} + y_{\min}) - y_0 = y_m - y_0$ means the output shift. As formula (15) was derived for a symmetric system, corresponding sustained oscillations with essential parameters are displayed in Fig. 4.

Assumption 1: Without loss of generality and also for simplicity, let $r = u_0 = \varepsilon = 0$ in the figure and hereinafter.

Define the difference $\Delta y_{rm} := y_m - r$. It holds for a symmetric system that $\Delta A = \Delta y_{rm}$; however, it does not hold for an asymmetric one, see Fig. 5.

Considering $\Delta A \neq \Delta y_{rm}$, computing (5), (6), or (10) yields erroneous results due to an incorrect evaluation of (13). It is worth noting that not only FF-based relay feedback identification methods can fail due to that, see, e.g., (15). The exponential decay method (introduced in Subsection II-B), which has been chosen as a representative of FF method in this study, requires the correct guess on y_0 due to computation of $y_a(t)$ in (7), see Fig. 6.

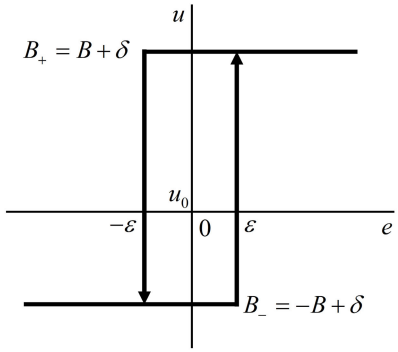

FIGURE 3. The static characteristics of a biased relay (with symmetric hysteresis).

These issues require modifying the standard relay test framework to estimate factual y_0 values for both subsystems $G_+(s)$, $G_-(s)$, as a system static or dynamic nonsymmetry cannot be excluded. Once this value is obtained, it is supposed

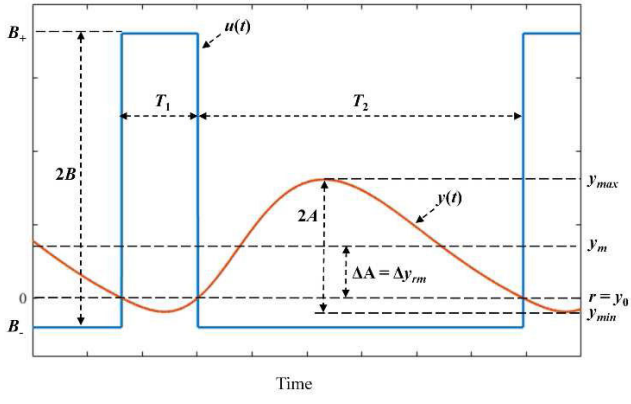

FIGURE 4. Sustained oscillations with relay (14) (without hysteresis) for a symmetric system.

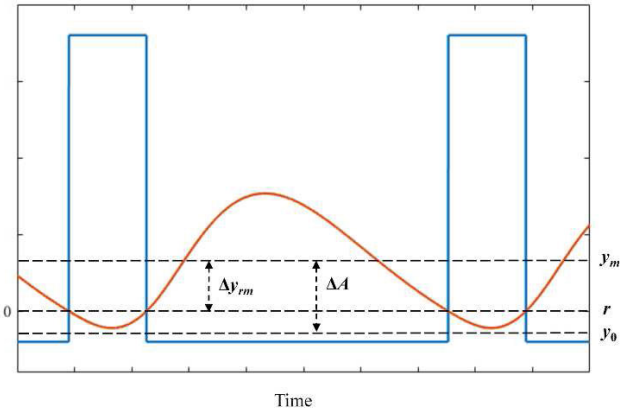

FIGURE 5. Sustained oscillations with relay (14) (without hysteresis) for an asymmetric system.

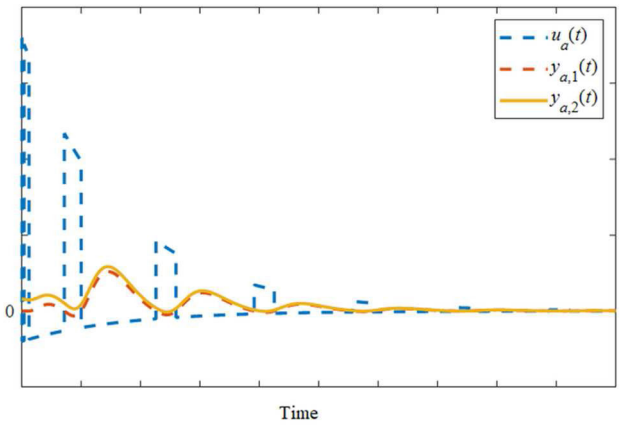

FIGURE 6. Exponentially decayed system input and output as per (7) and (13) for two different values of y_0 ($y_{0,1} = 0$, $y_{0,2} = -0.0794$), $a = 0.2$, see also Example 2.

that corresponding static and dynamic system properties are given by theoretical results (5) (or (10)) and (6), respectively.

IV. MAIN RESULT

Let us introduce two assumptions, the rationales of which are natural and meet theoretical expectations. The assumptions are crucial when deriving the main result and summarize already introduced facts.

Assumption 2: Let values of k and y_0 be known exactly for each subsystem $G_+(s)$, $G_-(s)$, satisfying (6) and (13). Then all other (dynamic) models' parameters are precisely given by (5) and/or (10) for any $\omega \neq 0$.

Assumption 3: The asymmetric identified system evinces different static and dynamic behavior (i.e., $G_+(s) \neq G_-(s)$) whenever the sign of $\Delta u(t)$ differs.

Assumption 2 expresses the idea that whenever the static gain is exactly found, then all the dynamic model parameters are also equal to those of the real-world system (in the case of perfect signal measurement and integral computations). Assumption 3 represents the "asymmetry" precondition for this research, i.e., a non-equal system response whenever the sign of the input excitation differs. Although it looks trivial and intuitive, it implies the idea of two separate experiments given below in the eventual algorithm.

The following proposition represents the cornerstone of the main result.

Proposition 1: Under Assumptions 1 and 2, it holds for the feedback identification test with relay (14) that

$$\Delta A = k\frac{u_{INT}}{T_{os}} = \frac{y_{INT}(y_0)}{T_{os}} \tag{16}$$

where $u_{INT} = T_1 B_+ + T_2 B_-$, $y_{INT}(y_0) = \int_0^{T_{os}} \Delta y(t+\tau)\,\mathrm{d}\tau$.

Proof: Under Assumption 1, it can be deduced from (6) that

$$k\int_0^{T_{os}} \Delta u(t+\tau)\,\mathrm{d}\tau = \int_0^{T_{os}} \Delta y(t+\tau)\,\mathrm{d}\tau$$
$$k\int_0^{T_{os}} \Delta u(t+\tau)\,\mathrm{d}\tau = y_{INT}(y_0) \tag{17}$$

It is clear from Fig. 4 that

$$u_{INT} := \int_0^{T_{os}} \Delta u(t+\tau)\,\mathrm{d}\tau = T_1 B_+ + T_2 B_- \tag{18}$$

Moreover, let the value of k be known exactly as per Assumption 2. The surface $y_{INT}(y_0)$ is considered relatively to y_0, and it can also be viewed as an equivalent rectangle area

$$y_{INT}(y_0) = (y_m - y_0)\,T_{os} = \Delta A T_{os} \tag{19}$$

Formula (16) is finally obtained by combining (17)-(19). ■

Remark 1: Proposition 1 can serve for computing k from the knowledge of ΔA, and vice versa, from (16). It is straightforward and effortless, mainly for symmetric systems, and the advantage of this result is that no information about the course or area of $y(t)$ is required when estimating k (compared to (6)), except for the knowledge of y_m.

Remark 2: The value of ΔA is usually only roughly estimated in literature, which may lead to erroneous results. For instance, $\Delta A \approx 0.5\,(B_+ + B_-)$ is used in [35].

The following theorem represents the core of the eventual relay-feedback parameter identification framework for asymmetric systems, i.e., the iterative formula for estimating the output operating point y_0, and the starting point for Assumption 2.

Theorem 1: Let k_+ and k_- be known exactly for $\Delta u > 0$ and $\Delta u < 0$, respectively. Consider that the corresponding operating point estimations are $\hat{y}_{0+}$ and $\hat{y}_{0-}$. Then the actual values of y_{0+} and y_{0-} are

$$y_{0\cdot} = \hat{y}_{0\cdot} + \Delta\hat{A}_{\cdot}(\hat{y}_{0\cdot}) - \Delta A_{\cdot} \tag{20}$$

where

$$\Delta A_{\cdot} := k_{\cdot}\frac{u_{INT\cdot}}{T_{osc\cdot}},$$
$$\Delta\hat{A}_{\cdot}(\hat{y}_{\cdot}) := \frac{y_{INT\cdot}(\hat{y}_{0\cdot})}{T_{osc\cdot}} \tag{21}$$

and the dot symbol $\cdot$ stands for $+$ or $-$.

Proof: The existence of two different pairs $\{y_{0+}, k_+\}$ and $\{y_{0-}, k_-\}$ is given by Lemma 2 and summarized in Assumption 3. Consider one of both asymmetric dynamics (e.g., $\Delta u > 0$), without loss of generality, with a guess $\hat{y}_{0+}$ and exactly known static gain k_+. If the guess is perfect, i.e., $\hat{y}_{0+} = y_{0+}$, then ΔA_+ can be calculated via (16) of Proposition 1 as either $\Delta A_+ = k_+ u_{INT+}/T_{os+}$ or $\Delta A_+ = y_{INT+}(y_{0+})/T_{os+}$. However, whenever the guess is imperfect, there exists an error

$$dA_+ = \Delta\hat{A}_{+,1} - \Delta\hat{A}_{+,2} = \frac{k_+ u_{INT+}}{T_{osc+}} - \frac{y_{INT+}\left(\hat{y}_{0+}\right)}{T_{osc+}} \tag{22}$$

As k_+ is exact, then $\Delta\hat{A}_{+,1} = \Delta A_+$ must be exact as well. The value of $\Delta\hat{A}_{+,2}$ depends on $\hat{y}_{0+}$. Hence, denote $\Delta\hat{A}_{+,2} = \Delta\hat{A}_+\left(\hat{y}_{0+}\right)$. If it is computed that $dA_+ > 0$, i.e., $\Delta A_+ > \Delta\hat{A}_+\left(\hat{y}_{0+}\right)$, it means that

$$\Delta\hat{A}_+\left(\hat{y}_{0+}\right) = \Delta A_+ - dA_+,\ dA_+ > 0 \tag{23}$$

which implies that the true value y_{INT+} must be higher than the estimate, see (21). Hence, the actual integral baseline y_{0+} should be lower than the estimate $\hat{y}_{0+}$, i.e.,

$$y_{0+} = \hat{y}_{0+} - \Delta\hat{y}_{0+}\ \Delta\hat{y}_{0+} > 0 \tag{24}$$

The output shift change equals the operating point correction, i.e., $dA_+ = \Delta\hat{y}_{0+}$. Considering this equality in (23) and (24), one can obtain (20) directly. ■

Corollary 1: Consider the current estimation pairs $\left\{{}^i\hat{k}_+, {}^i\hat{y}_{0+}\right\}$ and $\left\{{}^i\hat{k}_-, {}^i\hat{y}_{0-}\right\}$ for $\Delta u > 0$ and $\Delta u < 0$, respectively, that are sufficiently close to their true values. Then the updated estimations can be computed as

$${}^{i+1}\hat{y}_{0\cdot} = {}^i\hat{y}_{0\cdot} + \Delta\hat{A}_{\cdot,2}\left({}^i\hat{y}_{0\cdot}\right) - {}^i\Delta\hat{A}_{\cdot,1} \tag{25}$$

where

$${}^i\Delta\hat{A}_{\cdot,1} := {}^i\hat{k}_{\cdot}\frac{u_{INT\cdot}}{T_{osc\cdot}},$$
$$\Delta\hat{A}_{\cdot,2}\left({}^i\hat{y}_{0\cdot}\right) := \frac{y_{INT\cdot}\left({}^i\hat{y}_{0\cdot}\right)}{T_{osc\cdot}} \tag{26}$$

Proof: Iterative formula (25)-(26) results from Theorem 1. If the actual (true) static gain is not known, equality (20) does not hold as $\Delta A_\cdot$ in (23) is inexact. Therefore, it is assumed that $dA_\cdot \approx d\hat{A}_\cdot = \Delta\hat{y}_{0\cdot}$, which yields from (23), (24), and (26) that $y_{0\cdot} \approx \hat{y}_{0\cdot} + \Delta\hat{A}_{\cdot,2}\left(\hat{y}_{0\cdot}\right) - \Delta\hat{A}_{\cdot,1}$. It implies the iterative update (25) directly. ■

In accordance with Assumption 2, once sufficiently accurate static gain and output operating point estimations are found via Corollary 1, an FF-based technique can be applied to determine other model parameters. This one-step strategy can, however, be unsuitable as the update (25)-(26) may still lie far from the actual operating point.

Therefore, all system model parameters can be computed using (5) or (10), usually as a constrained nonlinear optimization problem for the current $\hat{y}_0$

$$\begin{aligned} \mathbf{p}^* &= \arg\min f(\mathbf{p}) \in R^n \\ f(\mathbf{p}) &:= \left\|\hat{\mathbf{g}} - \mathbf{g}_m(\mathbf{p})\right\| \\ s.t.: \mathbf{h}(\mathbf{p}) &\le \mathbf{0} \end{aligned} \tag{27}$$

where $\hat{\mathbf{g}} := \left[G(\mathrm{j}\omega_l + a)\right] \in R^M$, $l = \overline{0, M-1}$, is a vector, the entries of which are frequency points computed using (5) or (10), $\mathbf{g}_m(\mathbf{p}) := \left[G_m(\mathbf{p}, \mathrm{j}\omega_l + a)\right]$ are corresponding model points at the same frequencies, $\mathbf{p} \in R^n$ means the parameters' vector to be identified, and $\mathbf{h}(\mathbf{p})$ is a vector of constraints on the parameters due to model stability, feasibility, etc. The frequency set can be selected, e.g., as in (12); however, other possibilities exist (see Lemma 3 in Section V). In (27), the initial guess of model static gain is adopted from (26).

Once (27) is solved, the static gain estimation is updated via

$$\hat{k} = G_m\left(\mathbf{p}^*, s\right)\big|_{s=0} \tag{28}$$

that serves as the initial guess for (25)-(26) again.

This iterative framework approach can be summarized in the following algorithm (i.e., Algorithm 1) under Assumption 1 and using the FF method introduced in Subsection II-B. Possible modifications of Algorithm 1 are discussed in Subsection V-B.

Algorithm 1 Relay-Based Identification Strategy for Asymmetric Systems.

input: $G_{m+}(\mathbf{p}, s)$, $G_{m-}(\mathbf{p}, s)$
  for $j = 0, 1$
    select $B > 0,\ 0 < \delta < B$
    set $B_+ = B + (-1)^j\delta,\ B_- = -B + (-1)^j\delta$
    perform the test with relay (14)
    record $T_{os} = T_1 + T_2,\ u(t),\ y(t)$
    set ${}^0\hat{y}_0 = 0$
    compute the initial static gain guess ${}^0\hat{k}$ via (6)
    select $n_{iter}, a > 0, M > 0$
      $\omega_l \ge 0,\ l = \overline{0, M-1}$ (e.g., as per (12))
    for $i = \overline{1, n_{iter}}$
      select ${}^i\mathbf{p}_j$ reflecting ${}^{i-1}\hat{k}$
      substitute $y(t) \leftarrow \Delta y(t) = y(t) - {}^{i-1}\hat{y}_0$ in (7)
      compute $\hat{\mathbf{g}} := \left[G(\mathrm{j}\omega_l + a)\right]$ as per (10)
      ${}^i\mathbf{p}_m^* \leftarrow$**solve** (27)
      calculate ${}^i\hat{k}$ according to (28)
      update ${}^i\hat{y}_0$ as per (25)
    end
    return $\mathbf{p}_j^* \leftarrow {}^{n_{iter}}\mathbf{p}_j^*$
    end
output: $G_{m+}(\mathbf{p}, s)|_{\mathbf{p}=\mathbf{p}_0^*},\ G_{m-}(\mathbf{p}, s)|_{\mathbf{p}=\mathbf{p}_1^*}$

V. NUMERICAL COMPARATIVE STUDY

The reader is acquainted with a comparative numerical example in this section. Competitive methods used in this study are

concisely introduced first to understand the main numerical example description (Example 2). All the methods consider that $r = y_0$. In addition, some modifications and numerical aspects of Algorithm 1 are investigated.

A. COMPETITIVE METHODS OVERVIEW

The use of asymmetric relay with (symmetric) hysteresis represents the first competitive DF-based method [18], [19], [32]. Model parameters are evaluated based on (2) using the particular DF given by (15) with $\varepsilon > 0$. Let this method be labeled as METHOD-I. Artificial delays are applied to estimate more than one frequency point within this method [32], [33]. That is, the input-output delay element $G_a(s) = \exp\left(-\tau_{a,i}s\right)$ is placed in "Add" block in Fig. 2 where $i = \overline{1, n_\tau}$, $n_\tau = \lceil 0.5n - 1 \rceil$. Note that $|G_a(\mathrm{j}\omega_{os})| = 1$, $G_a(\mathrm{j}\omega_{os}) = -\tau_{a,i}\omega_{os}$.

A saturation relay with both symmetric and asymmetric settings is the second DF-based method [21], [44]. Let the former setting be labeled as METHOD-IIa, and the latter one (METHOD-IIb) should prove the advantage of an asymmetric system input level in the light of Assumption 3. The (asymmetric) saturation relay static characteristic is displayed in Fig. 7 and the corresponding DF is given by (29). The meaning of B and ΔA are the same as introduced below (14) and (15); see also Fig. 4. Again, the artificial delay is used in case that more than two model parameters are estimated.

$$N_{DF}\left(A, B, \Delta A, \overline{A}\right) = \frac{2B}{\pi}\left[\frac{1}{\overline{A}}\sin^{-1}\left(\frac{\overline{A}}{A}\right) + \sqrt{1-\left(\frac{\overline{A}}{A}\right)^2}\right]\sqrt{1-\left(\frac{\Delta A}{A}\right)^2} \tag{29}$$

The third DF method (METHOD-III) to be compared is a technique based on the output drift compensation followed by an asymmetric input excitation [40]. The method combines a symmetry restoration using a series of low-pass (given by filtering delay τ_F) and high-pass filtering, followed by a specific relay-based test. First, a block displayed in Fig. 8 to remove disturbances is placed instead of "Add" (see Fig. 2).

Then, the following excitation signal is injected into the system in the open loop

$$u = u_0 + \delta + u_r(\omega_{os}) + u_s(\omega_{low}) \tag{30}$$

to estimate multiple frequency points of the process where δ is a step change, $u_r(\omega_{os})$ represents a high-frequency part obtained as process-input sustained oscillations from the feedback-relay test, and $u_s(\omega_{low})$, $\omega_{low} = 0.5\omega_{os}$, expresses a low-frequency part having the form of a (symmetric) periodic square wave. Finally, the test data gives rise to a two-frequency-point parameter estimation of the first-order-plus-time-delay (FOPTD) system model

$$G_m(s) = G_{m,0}(s)\exp(-s\tau_m) = \frac{k}{Ts+1}\exp(-s\tau_m) \tag{31}$$

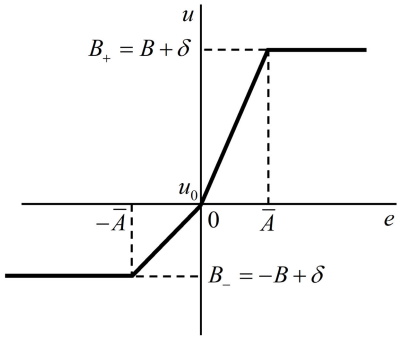

FIGURE 7. The static characteristics of an (asymmetric) saturation relay.

FIGURE 8. The "Add" block to remove disturbances [40].

The following formulae are based on the result derived in [45], which was extended in [40] to capture also the low-frequency dynamics of the process

$$\begin{aligned}
G_m(s) &= G_{m,0,low}(s)\exp\left[-s\left(\tau_{m,low} + \Delta\tau_m\right)\right],\\
\Delta\tau_m &= \frac{G_{m,os}(\mathrm{j}\omega_{os}) - G_{m,low}(\mathrm{j}\omega_{os})}{\omega_{os}},\\
G_{m,0,\cdot}(s) &= \frac{k_{m,\cdot}}{T_{m,\cdot}s+1},\ T_{m,\cdot} = \frac{\chi(\omega_\cdot)}{\omega_\cdot},\\
k_{m,os} &= k_{m,low} = \hat{G}(0),\\
\tau_{m,\cdot} &= \frac{\hat{G}(\mathrm{j}\omega_\cdot) - \tan^{-1}[\chi(\omega_\cdot)]}{\omega_\cdot},\\
\chi(\omega_\cdot) &= \sqrt{\frac{k_m^2}{\left|\hat{G}(\mathrm{j}\omega_\cdot)\right|^2} - 1},\\
\measuredangle G_{m,\cdot}(\mathrm{j}\omega_{os}) &= G_{m,0,\cdot}(\mathrm{j}\omega_{os}) - \tau_{m,\cdot}\omega_{os}
\end{aligned} \tag{32}$$

where the dot symbol stands for *os* or *low*. Readers are referred to [40] for more detail.

Two FF-based methods are benchmarked as well. A combination of the use of artificial delay and the n-shifting technique for asymmetric relay (14) is taken as the first one (METHOD-IV) [32]. The main idea is that multiple frequency points of the process are estimated at sustained oscillation frequencies $\omega_{os,l} \geq 0$, $l = 1, 2, \ldots$, so that the induced phase lag caused by the artificial delay decreases the value of $\omega_{os,l}$ as the process phase shift is higher than $-\pi$, see (2). Contrariwise, the n-shifting technique can multiply the frequency of the recorded oscillation data by an integer value. Namely, let periodic signal $y(t)$ have the period T_{os} and corresponding angular frequency $\omega_{os} = 2\pi/T_{os}$. Then the following signal

$$y_n(t) = \sum_{i=0}^{n-1} y\left(t - \frac{iT_{os}}{n}\right) \tag{33}$$

has the period of $T_{n,os} = T_{os}/n$ and frequency $\omega_{n,os} = n\omega_{os}$.

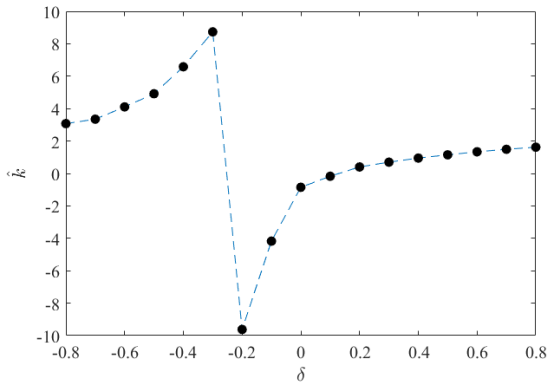

FIGURE 9. Computed relation between the selected relay asymmetry and computed static gain estimation.

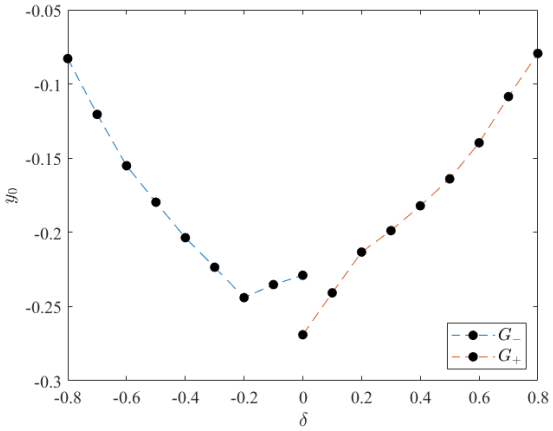

FIGURE 10. Relations between the selected relay asymmetry and true values of y_0 for known static gains.

The eventual signals are evaluated using formula (5). Besides, the relay asymmetry can suitably adjust the process input (i.e., the relay output) signal polarity.

Finally, a relay test for the FOPTD model with a special activation function represents the last competitive method (METHOD-V) [18]. Note that the activation function of type II is used in this research, which means a relay-feedback test followed by another relay-feedback test that applies a setpoint change to get better static gain estimation. As the obtained sustained oscillation evaluation includes a bunch of successive equations, details are omitted.

B. NUMERICAL EXAMPLES

Prior to providing readers with the motivation and the main simulation examples, let us concisely discuss the selection of frequencies for (5) and (10). As mentioned above, options $\omega_l = 0$ or $\omega_l = \omega_{os}$ are mostly used in the former case and formula (12) for the latter one. However, if (5) works for $\omega_l = 0$ (see (6)), it can also work for other frequencies. Similarly, (10) represents a general theoretical frequency response of the decayed (integrable) signal, and the DTFT formula (11) can be viewed as its simple quadrature. Hence, it can be used not only for (12) that returns frequencies less than half of the ultimate frequency ω_u (i.e., $G(\mathrm{j}\omega_u) = -1$). The following minor lemma represents guidance on selecting linearly increasing frequencies around ω_u (including ω_u).

Lemma 3: Consider vector ω of M linearly increasing frequencies $\omega = (\omega_1, \omega_2, \ldots, \omega_u, \ldots, \omega_{M-1}, \omega_M)$ that includes ω_u. Let M be given and select the position $1 \leq i_u \leq M$ such that $\omega_u = \omega_{i_u}$. Then the formula $\omega_i = ai + b$, $i = \overline{1, M}$, generating ω reads

$$a = \frac{(k_M - k_1)\,\omega_u}{M-1}, \quad b = k_1\omega_u - a \tag{34}$$

where:

a) If $i_u = 1$, then $k_1 = 1$ and $k_M = \omega_M/\omega_u > 1$ is selected.
b) If $i_u = M$, then $k_M = 1$ and $k_1 = \omega_1/\omega_u < 1$ is selected.
c) If $1 < i_u < M$, then

$$k_1 = k_M - \frac{(k_M - 1)\,(M-1)}{M - i_u} \tag{35}$$

and $k_M = \omega_M/\omega_u > 1$ is selected so that $k_1 \geq 0$.

Proof: The proof is based on a straightforward calculation of interpolation conditions $\omega_1 = a + b$, $\omega_u = ai_u + b$, $\omega_M = aM + b$, and auxiliary relations $\omega_1 = k_1\omega_u$, $\omega_M = k_M\omega_u$. As the interpolation set is overfitting, one of the parameters k_1, k_M can be selected (almost) freely. The rest of the proof is omitted. ■

The following introductory and motivating example demonstrates the relation between the choice of asymmetry δ of relay (14) and the true value of y_0 yielding the correct static gain from (6) and (13). Moreover, it elucidates Lemma 2 and Assumption 3.

Example 1: Consider an asymmetric system described by transfer functions for each of the subsystems

$$\begin{aligned} G_+(s) &= \frac{30}{s^4 + 8s^3 + 24s^2 + 32s + 15}, \\ G_-(s) &= \frac{200}{s^4 + 12s^3 + 54s^2 + 108s + 80} \end{aligned} \tag{36}$$

i.e., corresponding static gains and subsystem poles are $k_+ = 2$, $k_- = 2.5$ and $s_{+,i} = \{-1, -3, -2 \pm \mathrm{j}\}$, $s_{-,i} = \{-2, -4, -3 \pm \mathrm{j}\}$, respectively. The relation between δ (for $B = 1$) and the static gain estimation $\hat{k}$ computed using (6) when assuming $y_0 = r = 0$ is displayed in Fig. 9. Clearly, higher values of δ yield better estimation of k_+, and the lower δ is, the better guess on k_- is received. On the contrary, the estimation fails if the relay is close to its symmetry.

From the first sight, the course of relation $\delta \mapsto \hat{k}$ may serve for computing true values of both static gains. However, it is not so straightforward in practice due to several reasons. Firstly, it is necessary to evaluate many points $\hat{k}(\delta)$ for a possible extrapolation. Secondly, the computed extrapolation (approximation) function may not have a finite limit or its parameters can be erroneous. Thirdly, it is often impossible to reach sustained oscillation for higher values of $|\delta|$. However, it may be an alternative way to get an initial guess on $\hat{k}_+$, $\hat{k}_-$ and corresponding y_{0+}, y_{0-} (see Theorem 1).

Two separate relations between the selected relay asymmetry and computed y_{0+}, y_{0-} for the perfect knowledge of k_+, k_- as per (6) and (13) are displayed in Fig. 10. Apparently, the higher the value of $|\delta|$ is, the closer y_0 to r (except for the symmetric and almost symmetric relay settings). Nevertheless, the displayed courses do not indicate steady states of extrapolated data.

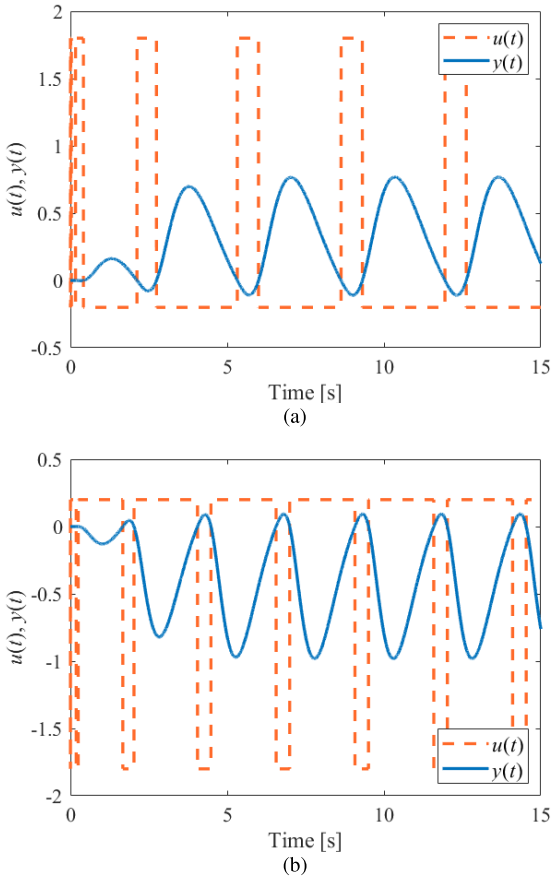

FIGURE 11. Relay feedback tests with sustained oscillations for settings $\{B_+, B_-\} = \{1.8, -0.2\}$ (a) and $\{B_+, B_-\} = \{0.2, -1.8\}$ (b).

Both the figures numerically validate Lemma 2 and provide a rationale for Assumption 3 and the necessity of asymmetric relay tests for sufficiently high values of $|\delta|$. However, one has to be careful about the disappearance of sustained oscillations.

Now, the main example demonstrating Algorithm 1 and comparing the results of other methods follows.

Example 2: Let the identified asymmetric process have transfer functions (36). Perform two separate relay feedback tests for the settings $B = 1, \delta = 0.8$ in Algorithm 1 (i.e., $B_+ = 1.8, B_- = -0.2$ and $B_+ = 0.2, B_- = -1.8$), under Assumption 1, see Fig. 11. Note that periods and angular frequencies of sustained oscillations are $T_{os+} = 3.313$s, $T_{os-} = 2.514$s and $\omega_{os+} = 1.897$ rad $\cdot$s^{-1}, $\omega_{os-} = 2.499$rad $\cdot$s^{-1}, respectively. Let the model have the same

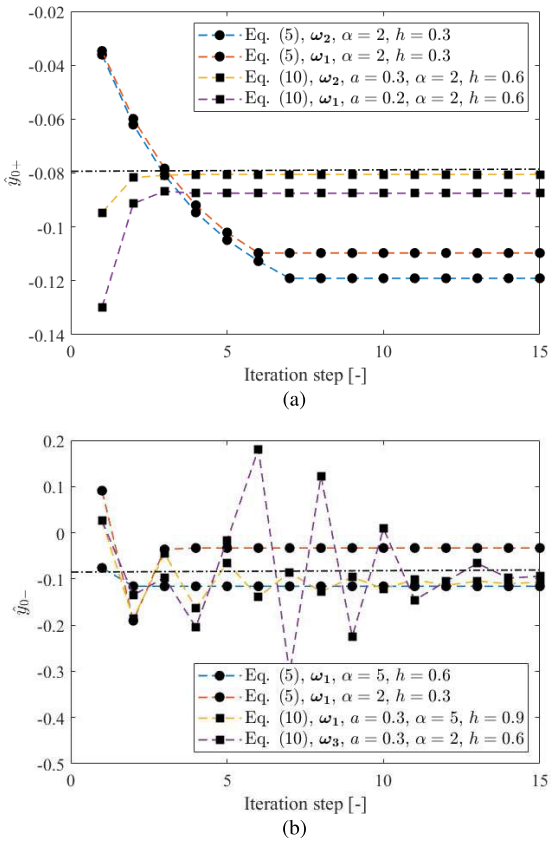

FIGURE 12. Iterated values of the setpoint estimates for selected settings using Algorithm 1 for G_+ with $\{B_+, B_-\} = \{1.8, -0.2\}$ (a) and G_- with $\{B_+, B_-\} = \{0.2, -1.8\}$.

dynamics as the true process (for simplicity)

$$G_m(s) = \frac{b_0}{s^4 + a_3 s^3 + a_2 s^2 + a_1 s + a_0} \tag{37}$$

except for the FOPTD model for some competitive methods.

For the default initial guess on the output operating point, ${}^0\hat{y}_0 = 0$, the corresponding static gain estimates are ${}^0\hat{k}_+ = 1.6205$, ${}^0\hat{k}_- = 3.0747$, in accordance with Fig. 9 and formula (6). The initial parameter set is selected to be stable with a unit static gain as ${}^0\mathbf{p} = ({}^0b_0, {}^0a_3, {}^0a_2, {}^0a_1, {}^0a_0) = (2, 2, 4, 4, 2)$.

We select three frequency sets. Namely, the first set $\omega_1 = (0 = \omega_{0,1}, \ldots, \omega_{19,1})$ is computed using (12) [36], [43]. The two others ω_2, ω_3 are computed using Lemma 3 for the settings $i_{u,2} = 18$, $k_{19,2} = 1.1$ and $i_{u,3} = 10$, $k_{19,3} = 2$, respectively, with $\omega_{2,0} = \omega_{3,0} = 0$. Moreover, consider frequency points evaluation using both formulae (5) and (10) (for a particular setting of a).

The optimization problem (27) is specifically defined as a constrained task with $p_i > 0, i = \overline{2,5}$, due to the necessary stability conditions governed by the following cost function,

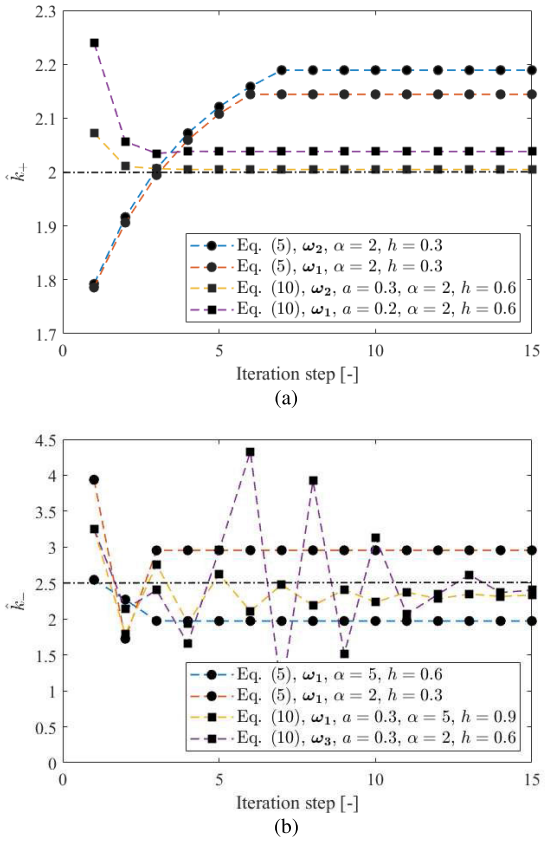

FIGURE 13. Iterated values of the static gain estimates for selected settings using Algorithm 1 for G_+ with $\{B_+, B_-\} = \{1.8, -0.2\}$ (a) and G_- with $\{B_+, B_-\} = \{0.2, -1.8\}$.

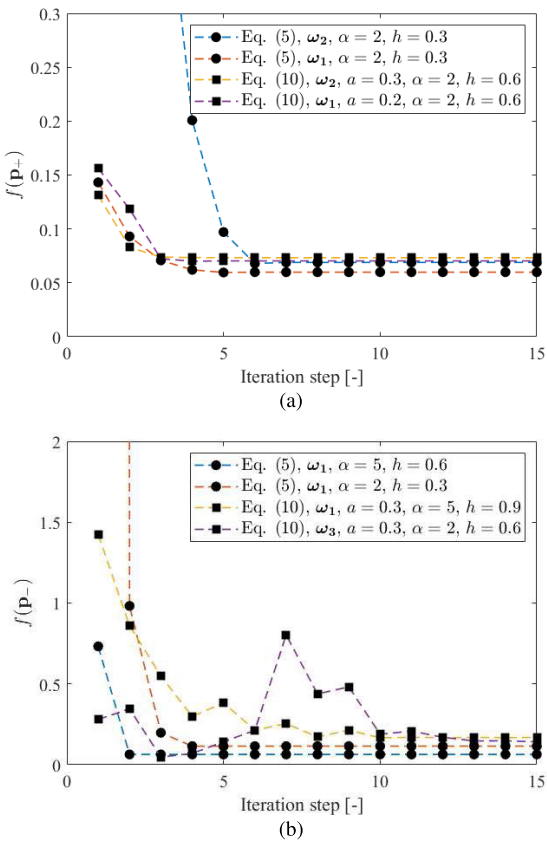

FIGURE 14. Iterated values of $f(\mathbf{p})$ for selected settings using Algorithm 1 for G_+ with $\{B_+, B_-\} = \{1.8, -0.2\}$ (a) and G_- with $\{B_+, B_-\} = \{0.2, -1.8\}$.

including a penalty function $\pi(\mathbf{p})$

$$\mathbf{p}^* = \arg\min_{\mathbf{p}} \left[\underbrace{\left\| \hat{\mathbf{g}} - \mathbf{g}_m(\mathbf{p}, \omega_i) \right\|_2}_{f(\mathbf{p})} - \alpha \underbrace{\sum_{j=2}^{5} \log\left(1 - \exp\left(p_j\right)\right)}_{\pi(\mathbf{p})} \right]$$
$$i = \overline{1, 20} \tag{38}$$

Subtask (38) of Algorithm 1 is solved using the well-established Nelder-Mead simplex method [46]. Here, the very basic setting of control parameters is made (i.e., the expansion, contraction, and reduction coefficients are 2, 0.5, and 0.5, respectively); however, several values of the initial simplex edge length within the range $h \in [0.1, 1]$ are selected. Besides, the weight on the penalty function varies as $\alpha \in [0.01, 5]$.

Iterated values of $\hat{y}_0$ for selected (best) results (from tenths of tests) are given in Fig. 12. Note that the true values $y_{0+} = -0.0794$, $y_{0-} = -0.0829$ (in accordance to Fig. 10) are indicated by dash-dot lines. The corresponding data for $\hat{k}$ and $f(\mathbf{p})$ are displayed in Figs. 13 and 14, respectively. Note that values of $f(\mathbf{p})$ are normed for comparison due to a different number of samples for (5) and (10)-(11). Besides, the values depend on a particular frequency set.

It is evident from the figures that the static gain estimation using (10) in Algorithm 1 is more accurate than that using formula (5), yet it requires a higher number of iteration steps for $\hat{k}_-$. Contrariwise, the frequency point fitting measured via $f(\mathbf{p})$ seems worse.

Let the eventual models obtained from Algorithm 1 for different settings be denoted by $G_{m,A-1}$, $G_{m,A-2}$, $G_{m,A-3}$, and $G_{m,A-4}$ (for both the subsystems) in the same order as introduced in the legend to Figs. 12-14.

We also perform identification tests with the same settings for the fixed value $y_0 = r = 0$ (i.e., without an update of $\hat{y}_0$) for comparison. The corresponding transfer functions are denoted by $G_{m,0-1}$, $G_{m,0-2}$, $G_{m,0-3}$, and $G_{m,0-4}$.

Regarding METHOD-I, the asymmetric relay with hysteresis has the following settings: $B = 1$ with $\delta = 0.8$ (for G_{m+}) and $\delta = -0.8$ (for G_{m-}), and $\varepsilon = 0.05$. Two artificial delays are chosen $\tau_a = \{0.2, 0.4\}$s. The computed three frequency points (i.e., $M = 3$) are used for model parameter estimation by minimizing (38) with (2) and (15) via the Nelder-Mead method again.

Among a multitude of tested settings, the following ones give the significant (best) results: $\alpha = 2, h = 0.3$ (giving rise to $G_{m+,I-1}$), $\alpha = 5, h = 0.9$ ($G_{m+,I-2}$), $\alpha = 2, h = 0.4$ ($G_{m-,I-1}$), and $\alpha = 5, h = 0.9$ ($G_{m-,I-2}$).

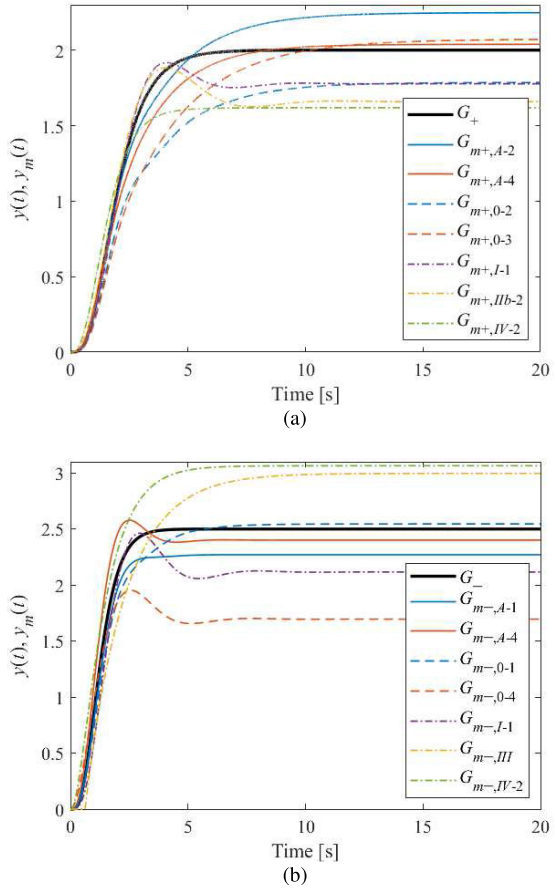

FIGURE 15. Comparison of unit step responses for non-normed subsystems G_+ (a) and G_- (b) and their models.

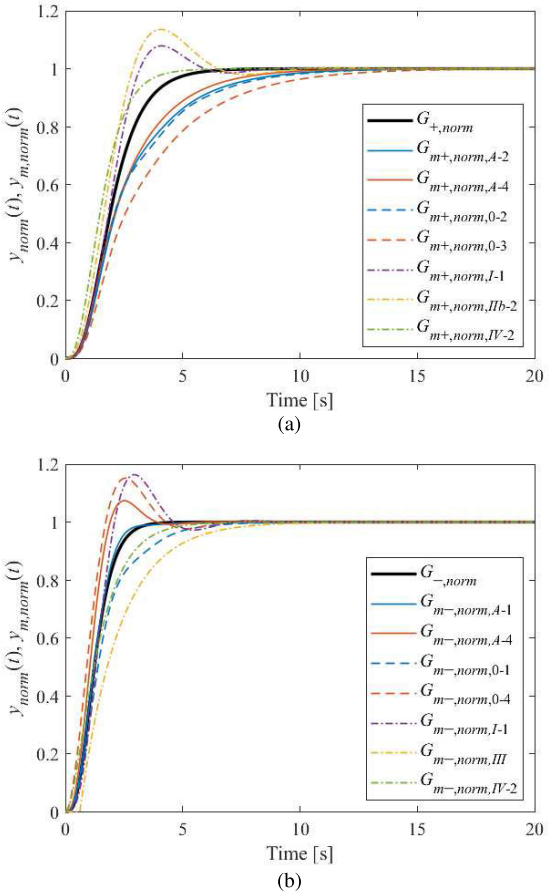

FIGURE 16. Comparison of unit step responses for normed subsystems G_+ (a) and G_- (b) and their models.

METHOD-IIa applies the symmetric relay (Fig. 7) with saturation ($B = 1$, $\delta = 0$), and METHOD-IIb adopts two asymmetric tests ($B = 1$, $\delta = \pm 0.8$). The same artificial delay values as in METHOD-I are taken. Again, conditions (2) for three oscillation frequencies are considered when minimizing (38) with (2) and (29). The selected optimization algorithm settings and corresponding eventual models for the symmetric tests are as follows: $\alpha = 2, h = 0.6$ (giving rise to $G_{m+,IIa-1}$ and $G_{m-,IIa-1}$) and $\alpha = 5, h = 0.6$ ($G_{m+,IIa-2}$, $G_{m-,IIa-2}$). The asymmetric tests are evaluated with the identical settings yielding $G_{m+,IIb-1}$, $G_{m-,IIb-1}$, $G_{m+,IIb-2}$, and $G_{m-,IIb-2}$.

METHOD-III is performed with the following settings of (30): $\delta = \pm 1/3$, $\omega_{os} = 2.795$ rad $\cdot s^{-1}$, $\omega_{low} = 1.3975$ rad $\cdot s^{-1}$. The resulting models are denoted by $G_{m+,III}$ and $G_{m-,III}$ for $\delta = 1/3$ and $\delta = -1/3$, respectively.

The setting of METHOD-IV takes one artificial delay $\tau_a = 0.4$s to decrease the sustained oscillation frequency and 2-shifting and 3-shifting techniques to get frequency integer multiples as per (33). Moreover, the asymmetric relay (without hysteresis) with the same settings as in Algorithm 1 is used. Then, all the obtained signals are subject to (5), and the fitting of all the estimated (computed) frequency points is made using (38) for $M = 5$ and the Nelder-Mead method. The selected optimization method settings and corresponding obtained model notations are as follows: $\alpha = 2, h = 0.3$ (giving rise to $G_{m+,IV-1}$ and $G_{m-,IV-1}$), $\alpha = 5, h = 0.9$ ($G_{m+,IV-2}$), and $\alpha = 5, h = 0.6$ ($G_{m-,IV-2}$).

Finally, the activation stage of METHOD-V adopts the asymmetric relay with the same setting as above, followed by the symmetric on-off relay. The resulting FOPTD models are denoted by $G_{m+,V}$ and $G_{m-,V}$.

The eventual transfer function models of subsystems G_+ and G_- are provided to the reader in Table 1 and Table 2, respectively. Tables 3 and 4 display performance metrics for both the subsystems and their models given in Table 1 and Table 2 in time- and frequency-domains.

The metrics are defined as follows:

$$\Delta k = \left|1 - \frac{k_m}{k}\right| = \left|1 - \frac{G_m(0)}{G(0)}\right| [\times 100\%] \tag{39}$$

$$\text{RMSE} = \sqrt{\frac{\sum_{i=0}^{\omega_{k,f}} \left|G(j\omega_{k,i}) - G_m(j\omega_{k,i})\right|^2}{N_k}} \tag{40}$$

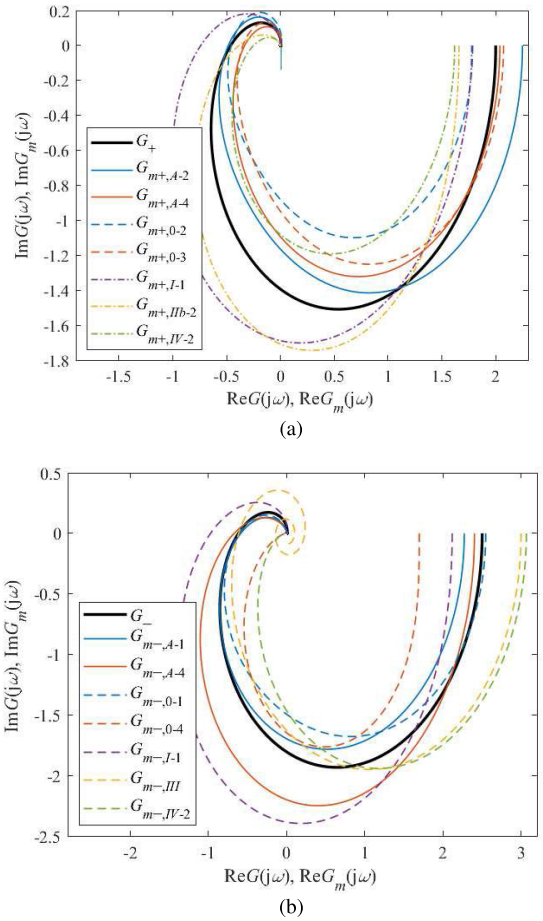

FIGURE 17. Comparison of Nyquist plots for non-normed subsystems G_+ (a) and G_- (b) and their models.

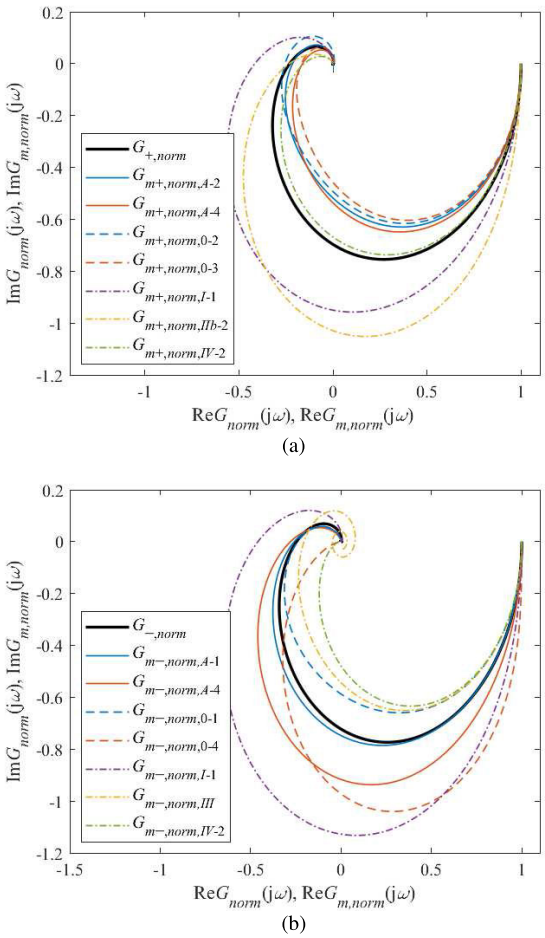

FIGURE 18. Comparison of Nyquist plots for normed subsystems G_+ (a) and G_- (b) and their models.

where k_m means the (eventual) model static gain, and $\omega_{k,i} \in \Omega_k$, $\omega_{1,f} = \omega_u$, $N_1 = |\Omega_1|$, $\omega_{2,f} = 3\omega_u$, $N_2 = |\Omega_2|$.

$$\begin{aligned} \mathrm{IAE}_{63} &= \int_0^{t_{63}} |y(t) - y_m(t)| \mathrm{d}t \\ &\approx T_s \sum_{i=0}^{N_{63}} |y(t_i) - y_m(t_i)| \end{aligned} \tag{41}$$

where $t_{63} := \{t : y(t) = k[1 - \exp(-1)]\} = N_{63}T_s$ and $y(t)$, $y_m(t)$ mean true and modelled step responses, respectively. Note that t_{63} corresponds to the time constant of the first-order system.

$$\begin{aligned} \mathrm{ITAE} &= \int_0^{\infty} t \left| y_{norm}(t) - y_{m,norm}(t) \right| \mathrm{d}t \\ &\approx T_s \sum_{i=0}^{N} t_i |y(t_i) - y_m(t_i)| \end{aligned} \tag{42}$$

where the subscript *norm* expresses the normed (unit static gain) step response. Note that (40) and (41) are also computed for the normed responses in Table 5 and Table 6.

The static gain error Δk and root-mean-squared errors (RMSEs) between system and model Nyquist plots for different frequency ranges $\Omega_1 := [0, \omega_u]$, $\Omega_2 := [0, 3\omega_u]$ are primary performance measures, where ω_u means the ultimate system frequency of a particular subsystem ($\omega_{u+} = 1.9997$ rad $\cdot$s^{-1}, $\omega_{u-} = 3.0006$rad $\cdot$s^{-1}). The integral absolute error (IAE_{63}) measures the matching of the step response transition part (i.e., until the value $y_{63} = k[1 - \exp(-1)]$ is reached).

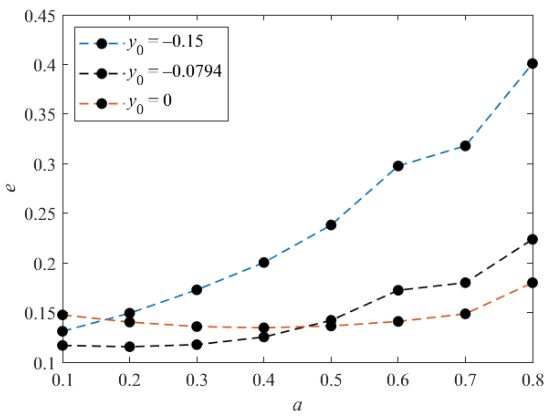

FIGURE 19. Relations between error e (43) and decaying exponent a (10) for a frequency set computed via (12) – Example 3.

TABLE 1. Computed models of G_+ (Example 2).

	Transfer function
Algorithm 1, (5)	$G_{m+,A-1}(s)=\frac{29.0815}{s^4+8.8295s^3+21.8029s^2+38.3777s+13.2854}$
	$G_{m+,A-2}(s)=\frac{27.6255}{s^4+8.0313s^3+20.2712s^2+35.0212s+12.2890}$
Algorithm 1, (10)	$G_{m+,A-3}(s)=\frac{31.7058}{s^4+7.4879s^3+26.1029s^2+41.7717s+15.8156}$
	$G_{m+,A-4}(s)=\frac{31.9219}{s^4+7.6641s^3+25.9764s^2+41.8680s+15.6603}$
$y_0=0$, (5)	$G_{m+,0-1}(s)=\frac{12.8128}{s^4+5.8210s^3+11.9405s^2+22.3909s+7.1486}$
	$G_{m+,0-2}(s)=\frac{16.2985}{s^4+5.9197s^3+14.4566s^2+26.6741s+9.1265}$
$y_0=0$, (10)	$G_{m+,0-3}(s)=\frac{16.6658}{s^4+6.2191s^3+16.8859s^2+28.1404s+8.0414}$
	$G_{m+,0-4}(s)=\frac{18.6952}{s^4+6.9039s^3+18.4036s^2+31.3156s+8.3456}$
METHOD-I	$G_{m+,I-1}(s)=\frac{28.5237}{s^4+10.8842s^3+23.9113s^2+27.8393s+16.0501}$
	$G_{m+,I-2}(s)=\frac{27.0719}{s^4+9.7371s^3+21.4989s^2+25.8051s+11.1721}$
METHOD-IIa	$G_{m+,IIa-1}(s)=\frac{804.8763}{s^4+82.6275s^3+284.0181s^2+604.9769s+260.6039}$
	$G_{m+,IIa-2}(s)=\frac{62.8734}{s^4+6.7617s^3+33.9493s^2+49.2122s+53.1854}$
METHOD-IIb	$G_{m+,IIb-1}(s)=\frac{172.6895}{s^4+35.5101s^3+150.0345s^2+141.2915s+120.1691}$
	$G_{m+,IIb-2}(s)=\frac{363167.9}{s^4+77535.24s^3+295862.7s^2+304590.4s+218942.3}$
METHOD-III	$G_{m+,III}(s)=\frac{1.5}{0.5691s+1}\exp(-0.8179s)$
METHOD-IV	$G_{m+,IV-1}(s)=\frac{2158.461}{s^4+300.5185s^3+1177.236s^2+2335.320s+1333.977}$
	$G_{m+,IV-2}(s)=\frac{9615.428}{s^4+1188.222s^3+5420.299s^2+9795.767s+5942.550}$
METHOD-V	$G_{m+,V}(s)=\frac{0.7445}{0.6841s+1}\exp(-1.3583s)$

As the performances' values are significantly affected by the error Δk, the metrics are computed for the normed (unit) static gain of both the model and system (see Table 5 and Table 6). In addition, the integral absolute time-weighted error (ITAE) of complete normed step responses is computed. The best results for using Algorithm 1, the fixed $y_0 = 0$ with (5) and (10), and the remaining competitive methods are highlighted in green; while the worst ones are in red.

It can be deduced from Table 3 and Table 5 that the proposed method governed by Algorithm 1 gives the best performance metrics for G_+, except for the ITAE criterion. This is mainly given by relatively slow normed unit step responses.

The use of (5) returns lower performance metric values than the exponential decay; however, computational experiments show that significantly more different optimization algorithm settings have to be examined to reach a satisfactory result.

It can be mainly seen that the static gain estimation is much worse if $y_0 = 0$ is considered (i.e., the data for all the methods except for the proposed one). If asymmetric process input is used (caused by a relay setting or an excitation signal), this estimation is better than using a symmetric input; compare, e.g., METHOD-IIa vs. METHOD-IIb. This finding agrees with Example 1.

For G_+, the DF-based methods (METHOD-I and METHOD-IIb) for non-normed data yield better results than the FF-based ones (except for ITAE again). This can stem from the fact that the DF-based methods do not explicitly rely on an accurate guess on y_0.

Contrariwise, METHOD-IV gives the best metrics' values for G_- in the frequency domain among the competitive

TABLE 2. Computed models of G_- (Example 2).

	Transfer function
Algorithm 1, (5)	$G_{m-,A-1}(s) = \frac{468.4745}{s^4 + 33.4057s^3 + 131.4869s^2 + 272.0617s + 206.2943}$
	$G_{m-,A-2}(s) = \frac{197.6120}{s^4 + 12.9284s^3 + 54.7164s^2 + 113.6170s + 66.8541}$
Algorithm 1, (10)	$G_{m-,A-3}(s) = \frac{49432.98}{s^4 + 2127.317s^3 + 9881.605s^2 + 19990.77s + 19953.91}$
	$G_{m-,A-4}(s) = \frac{1581.601}{s^4 + 68.6666s^3 + 330.3481s^2 + 645.1198s + 658.6492}$
$y_0 = 0$, (5)	$G_{m-,0-1}(s) = \frac{576.8627}{s^4 + 551.0339s^3 + 159.1295s^2 + 395.3166s + 226.6130}$
	$G_{m-,0-2}(s) = \frac{75.6309}{s^4 + 7.5675s^3 + 25.1960s^2 + 61.9871s + 23.8013}$
$y_0 = 0$, (10)	$G_{m-,0-3}(s) = \frac{9561.329}{s^4 + 26.5107s^3 + 812.0102s^2 + 9595.617s + 2940.568}$
	$G_{m-,0-4}(s) = \frac{34322.73}{s^4 + 8.2585s^3 + 9916.770s^2 + 14589.92s + 20238.51}$
METHOD-I	$G_{m-,I-1}(s) = \frac{73.6188}{s^4 + 8.0324s^3 + 28.3135s^2 + 37.5309s + 34.7844}$
	$G_{m-,I-2}(s) = \frac{11507.54}{s^4 + 1186.952s^3 + 4129.027s^2 + 5490.447s + 6413.183}$
METHOD-IIa	$G_{m-,IIa-1}(s) = \frac{804.8763}{s^4 + 82.6275s^3 + 284.0181s^2 + 604.9769s + 260.6039}$
	$G_{m-,IIa-2}(s) = \frac{62.8734}{s^4 + 6.7617s^3 + 33.9493s^2 + 49.2122s + 53.1854}$
METHOD-IIb	$G_{m-,IIb-1}(s) = \frac{203.5422}{s^4 + 24.6409s^3 + 111.9843s^2 + 153.1453s + 111.8174}$
	$G_{m-,IIb-2}(s) = \frac{191.7740}{s^4 + 16.8634s^3 + 88.7320s^2 + 98.3954s + 136.6040}$
METHOD-III	$G_{m-,III}(s) = \frac{2.9970}{1.6754s + 1}\exp(-0.6224s)$
METHOD-IV	$G_{m-,IV-1}(s) = \frac{9919.130}{s^4 + 5.835s^3 + 1671.309s^2 + 3982.497s + 3236.646}$
	$G_{m-,IV-2}(s) = \frac{783124.7}{s^4 + 1719.562s^3 + 127633.5s^2 + 381079.5s + 255536.3}$
METHOD-V	$G_{m-,V}(s) = \frac{0.7445}{0.6841s + 1}\exp(-1.3583s)$

TABLE 3. Computed performance values for G_{m+} (Example 2, Table 1).

	Δk [%]	RMSE (Ω_1)	RMSE (Ω_2)	IAE$_{63}$ [x10^{-2}]
$G_{m+,A-1}(s)$	9.45	0.1246	0.0720	6.5792
$G_{m+,A-2}(s)$	12.40	0.1159	0.0670	3.2280
$G_{m+,A-3}(s)$	0.28	0.1434	0.0831	8.3094
$G_{m+,A-4}(s)$	1.92	0.1398	0.0810	7.6791
$G_{m+,0-1}(s)$	10.38	0.2271	0.1318	30.660
$G_{m+,0-2}(s)$	10.71	0.2137	0.1237	23.580
$G_{m+,0-3}(s)$	3.62	0.2342	0.1354	28.787
$G_{m+,0-4}(s)$	12.01	0.2419	0.1398	27.268
$G_{m+,I-1}(s)$	11.14	0.1752	0.1015	7.9864
$G_{m+,I-2}(s)$	21.16	0.2000	0.1157	5.6964
$G_{m+,IIa-1}(s)$	54.43	0.3803	0.2226	86.510
$G_{m+,IIa-2}(s)$	40.89	0.4766	0.2779	35.478
$G_{m+,IIb-1}(s)$	28.15	0.2302	0.1335	5.0826
$G_{m+,IIb-2}(s)$	17.06	0.1726	0.1006	8.9546
$G_{m+,III}(s)$	25.00	0.4560	0.3526	42.048
$G_{m+,IV-1}(s)$	19.10	0.2443	0.1431	20.268
$G_{m+,IV-2}(s)$	19.10	0.2363	0.1389	22.999
$G_{m+,V}(s)$	62.78	0.4312	0.2744	75.413

TABLE 4. Computed performance values for G_{m-} (Example 2, Table 1).

	Δk [%]	RMSE (Ω_1)	RMSE (Ω_2)	IAE$_{63}$ [x10^{-2}]
$G_{m-,A-1}(s)$	9.16	0.1031	0.0707	6.5700
$G_{m-,A-2}(s)$	18.24	0.1997	0.1162	3.1667
$G_{m-,A-3}(s)$	0.91	0.3630	0.2139	26.643
$G_{m-,A-4}(s)$	3.95	0.3523	0.2073	23.871
$G_{m-,0-1}(s)$	1.82	0.1922	0.1218	12.654
$G_{m-,0-2}(s)$	27.10	0.4459	0.2641	23.539
$G_{m-,0-3}(s)$	30.06	0.6654	0.4524	25.095
$G_{m-,0-4}(s)$	32.16	0.4075	0.2685	13.751
$G_{m-,I-1}(s)$	15.34	0.6636	0.3847	23.313
$G_{m-,I-2}(s)$	28.23	0.7477	0.4326	17.657
$G_{m-,IIa-1}(s)$	23.54	0.4319	0.2641	22.879
$G_{m-,IIa-2}(s)$	52.71	0.5627	0.3359	37.520
$G_{m-,IIb-1}(s)$	27.19	0.4682	0.2956	37.231
$G_{m-,IIb-2}(s)$	43.85	0.4990	0.3045	25.562
$G_{m-,III}(s)$	19.80	0.3763	0.2489	29.918
$G_{m-,IV-1}(s)$	22.59	0.3182	0.2571	50.452
$G_{m-,IV-2}(s)$	22.59	0.2934	0.2544	38.819
$G_{m-,V}(s)$	70.22	1.0259	0.6546	83.345

methods. Surprisingly, a relay asymmetry does not improve time domain responses of non-normed models; however, a slight improvement can be observed for the normed data.

Based on Tables 3-6, representative models are selected for the eventual graphical comparison of time- and frequency domain plots.

Namely, model transfer functions $G_{m+,A-2}(s)$, $G_{m+,A-4}(s)$, $G_{m+,0-2}(s)$, $G_{m+,0-3}(s)$, $G_{m+,I-1}(s)$, $G_{m+,IIb-2}(s)$, and $G_{m+,IV-2}(s)$ represent the set for G_+, and $G_{m-,A-1}(s)$, $G_{m-,A-4}(s)$, $G_{m-,0-1}(s)$, $G_{m-,0-4}(s)$, $G_{m-,I-1}(s)$, $G_{m-,III}(s)$, and $G_{m-,IV-2}(s)$ is another set of models estimating G_-. Non-normed unit step responses are displayed in Fig. 15, while Fig. 16 provides readers with those for the normed (unit static gain) models. Analogously, Figs. 17 and 18 give a comparison of Nyquist plots.

C. POSSIBLE ALGORITHM MODIFICATIONS

Let us discuss possible modifications of Algorithm 1 and its setting. As the algorithm represents a framework rather than a method, it can be altered in several ways. In particular, any FF-based technique, the accuracy of which is significantly affected by a guess on y_0 can be applied within the algorithm. We have used the exponential decay method (see Subsection II-B) that includes the decaying exponent a as its crucial parameter. A bunch of numerical tests for various exponent settings have been made to obtain solutions

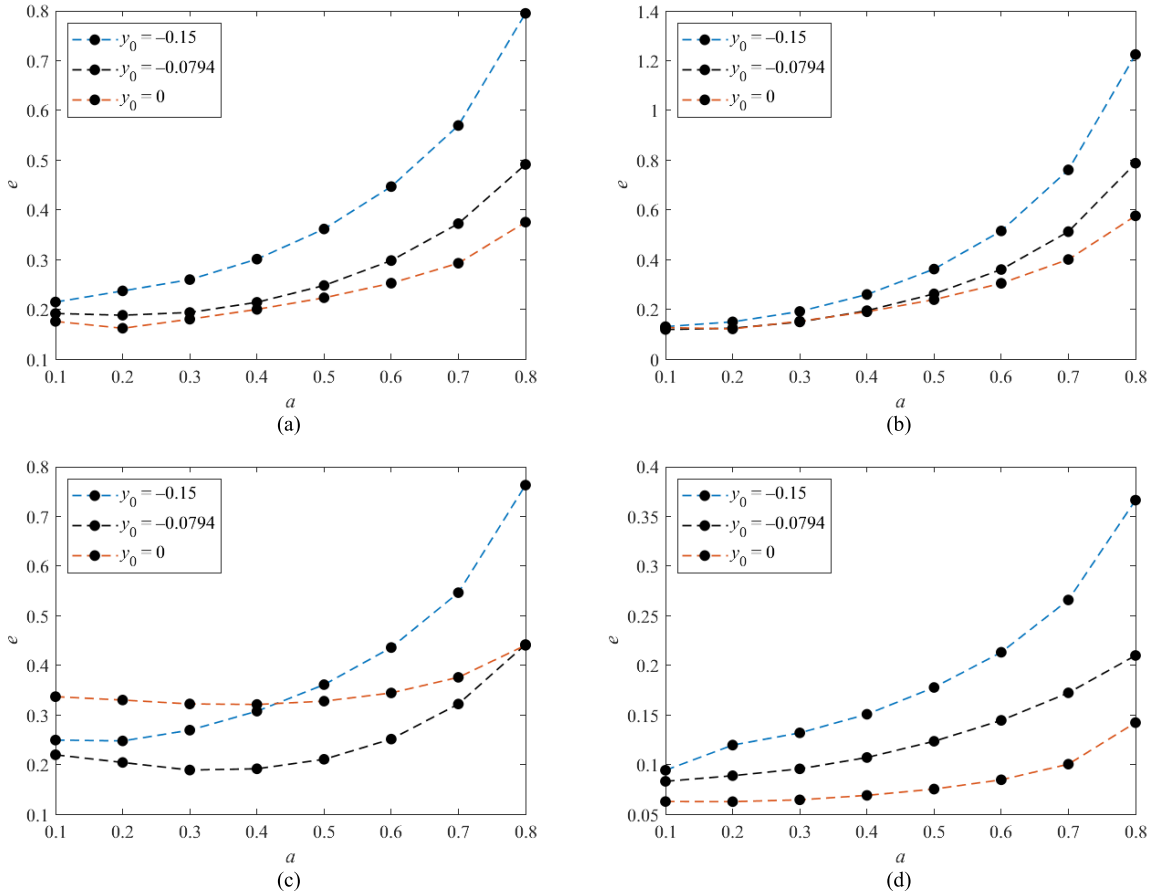

FIGURE 20. Relations between error e (43) and decaying exponent a (10) for a frequency set computed using Lemma 3 with $i_u = 10$, $k_1 = 0.55$, $k_{19} = 1.5$ (a) , $i_u = 11$, $k_1 = 0.78$, $k_{19} = 1.2$ (b), $i_u = 18$, $k_1 = 0.15$, $k_{19} = 1.1$ (c), $i_u = 2$, $k_1 = 0.89$, $k_{19} = 3$ (d) – Example 3.

presented in Example 2. One can take values suggested in literature [18], [43] as the initial setting; however, it can be tricky. Especially, a suitable (or the best) option depends on the frequency set ω_l, $l = \overline{1, M}$, in which the frequency points are computed (for instance, it is possible to consider rule (12) or take Lemma 3). The following numerical example attempts to elucidate these thoughts.

Example 3: Assume subsystem $G_+(s)$ in (36) and perform the relay-based experiment as in Example 2 (see Fig. 11(a)). Apply the exponential decay technique for $M = 20$, yet different sets of ω_l, several values of y_0, and various settings of a in (10)-(11), (13). Recall that the exact operation point reads $y_0 = -0.0794$. Define the following error

$$e = \frac{1}{M} \sum_{i=0}^{M-1} \left| \hat{G}(\mathrm{j}\omega_i + a) - G(\mathrm{j}\omega_i + a) \right| \qquad (43)$$

where points $\hat{G}(\cdot)$ are computed via (10)-(11), (13), and $G(\cdot)$ represent true process values.

Errors (43) for the frequency set computed via (12) (for $M = 20$) are displayed in Fig. 19. In Fig. 20, the same is done for four sets calculated via Lemma 3 (the value of $M = 19$ is taken in (34)-(35), including $\omega_0 = 0$). Namely, "wide" ($i_u = 10$, $k_1 = 0.55$, $k_{19} = 1.5$), "narrow" ($i_u = 11$, $k_1 = 0.78$, $k_{19} = 1.2$), "low-frequency" ($i_u = 18$, $k_1 = 0.15$, $k_{19} = 1.1$), and "high-frequency" ($i_u = 2$, $k_1 = 0.89$, $k_{19} = 3$) ranges are selected for the comparison.

Some settings return error minima very close to zero (Figs. 20(b), 20(d)), which is unsuitable as the final value of the decayed signal is too high. More critically, some frequency sets yield lower error for the initial (incorrect) operation point $y_0 = 0$ that for the correct one $y_0 = -0.0794$.

This effect is unacceptable since Algorithm 1 can return the optimization problem solution with a lower cost function value (27) for an erroneous guess on y_0 that, moreover, can be evaluated as the eventual operating point. Then, the static gain estimation can also fail. Therefore, the options on Fig. 19 and Fig. 20(c) seem to be preferable. It implies that the selected frequency set for the exponential decay method should include sufficiently low values, not exceeding the ultimate frequency to a large extent.

A suitable choice of M represents another issue. The higher the value is, the higher the computational effort and time are. On the contrary, a low number of frequency points to be fitted may lead to insufficient accuracy of the identified model.

TABLE 5. Computed performance values for normed G_{m+} (Example 2).

	ITAE	RMSE (Ω_1)	RMSE (Ω_2)	IAE$_{63}$ [x10^{-2}]
$G_{m+,A-1}(s)$	374.19	0.0623	0.0360	3.2896
$G_{m+,A-2}(s)$	351.24	0.0580	0.0335	1.6140
$G_{m+,A-3}(s)$	237.51	0.0717	0.0416	4.1550
$G_{m+,A-4}(s)$	253.68	0.0699	0.0405	3.8396
$G_{m+,0-1}(s)$	515.70	0.0876	0.0659	15.330
$G_{m+,0-2}(s)$	399.34	0.1069	0.0619	11.790
$G_{m+,0-3}(s)$	712.18	0.1171	0.0677	14.394
$G_{m+,0-4}(s)$	877.72	0.1210	0.0699	13.634
$G_{m+,I-1}(s)$	170.55	0.0876	0.0508	3.9930
$G_{m+,I-2}(s)$	46.224	0.1000	0.0580	2.8480
$G_{m+,IIa-1}(s)$	158.42	0.1902	0.1113	11.439
$G_{m+,IIa-2}(s)$	121.18	0.2383	0.1390	18.760
$G_{m+,IIb-1}(s)$	414.04	0.1151	0.0668	2.5413
$G_{m+,IIb-2}(s)$	300.10	0.0863	0.0503	4.4773
$G_{m+,III}(s)$	185.21	0.3093	0.2389	44.298
$G_{m+,IV-1}(s)$	78.519	0.1222	0.0716	10.134
$G_{m+,IV-2}(s)$	114.60	0.1182	0.0695	11.500
$G_{m+,V}(s)$	99.400	0.2156	0.1372	37.707

TABLE 6. Computed performance values for normed G_{m-} (Example 2).

	ITAE	RMSE (Ω_1)	RMSE (Ω_2)	IAE$_{63}$ [x10^{-2}]
$G_{m-,A-1}(s)$	10.952	0.0412	0.0283	2.6280
$G_{m-,A-2}(s)$	92.228	0.0799	0.0465	1.2667
$G_{m-,A-3}(s)$	69.509	0.1452	0.0856	10.657
$G_{m-,A-4}(s)$	75.909	0.1409	0.0829	9.5485
$G_{m-,0-1}(s)$	119.34	0.0769	0.0487	5.0618
$G_{m-,0-2}(s)$	457.05	0.1784	0.1056	9.4155
$G_{m-,0-3}(s)$	910.74	0.2662	0.1810	10.038
$G_{m-,0-4}(s)$	149.38	0.1630	0.1074	5.5003
$G_{m-,I-1}(s)$	137.22	0.2654	0.1539	9.3253
$G_{m-,I-2}(s)$	260.14	0.2991	0.1730	9.1515
$G_{m-,IIa-1}(s)$	315.09	0.1728	0.1056	11.439
$G_{m-,IIa-2}(s)$	124.90	0.2251	0.1344	15.008
$G_{m-,IIb-1}(s)$	81.983	0.1873	0.1182	14.893
$G_{m-,IIb-2}(s)$	313.47	0.1996	0.1218	10.225
$G_{m-,III}(s)$	289.56	0.1716	0.1065	15.550
$G_{m-,IV-1}(s)$	17.246	0.1273	0.1028	20.181
$G_{m-,IV-2}(s)$	66.744	0.1174	0.1018	15.528
$G_{m-,V}(s)$	117.22	0.4104	0.2618	33.338

Last but not least, the selection of an optimization technique solving problem (27) (or (38)) is a challenging task. For instance, modern metaheuristic approaches [47] might be benchmarked in the future research.

VI. CONCLUSION

This research has presented a novel framework for relay-based parameter identification techniques for asymmetric systems and processes. It has attempted to provide the reader with a rationale for two asymmetric tests giving rise to two different operating points for both asymmetric subsystems. An algorithm estimating static and dynamic parameters has been proposed as the main results. The algorithm efficacy and reasonability have been demonstrated via a detailed comparative example, in which some other competitive methods considering the unique operating point have been benchmarked. The main example has proved a necessity of an accurate guess on the operating point for frequency-based relay feedback identification methods. A concise discussion on possible framework modifications and setting have also been given, yielding a possible future research focus.

In future research, two research tasks should mainly be investigated. First, a practical (laboratory) verification of the proposed framework using a suitable asymmetric process ought to be made. Second, the identification data can be contaminated by noise, and the proposed method should be verified with the polluted data. As real-life systems and processes are inherently affected by noise and disturbances, both tasks can be performed simultaneously. In addition, a benchmark test with disturbance attenuation methods that have not been covered in this research might be made.

REFERENCES

[1] D.-W. Zhang, Y.-L. Chen, G.-Q. Zhang, L.-J. Lang, Z. Li, and S.-L. Zhu, "Skin superfluid, topological Mott insulators, and asymmetric dynamics in an interacting non-Hermitian Aubry-André-Harper model," *Phys. Rev. B, Condens. Matter*, vol. 101, no. 23, Jun. 2020, Art. no. 235150.

[2] Y. Zushi and K. A. Takeuchi, "Scaling and spontaneous symmetry restoring of topological defect dynamics in liquid crystal," *Proc. Nat. Acad. Sci. USA*, vol. 119, no. 41, Oct. 2022, Art. no. e2207349119.

[3] R. Han, A.-M. Zhang, S. Tan, and S. Li, "Interaction of cavitation bubbles with the interface of two immiscible fluids on multiple time scales," *J. Fluid Mech.*, vol. 932, Dec. 2021, Art. no. 976.

[4] M. Chen, A. Wang, C. Wang, H. Wu, and B. Bao, "DC-offset-induced hidden and asymmetric dynamics in memristive Chua's circuit," *Chaos, Solitons Fractals*, vol. 160, Jul. 2022, Art. no. 112192.

[5] A. Vasičkaninová, M. Bakošová, and A. Mészáros, "Fuzzy control design for energy efficient heat exchanger network," *Chem. Eng. Trans.*, vol. 88, pp. 529–534, Nov. 2021.

[6] I. Rodriguez and A. Campo, "Numerical investigation of forced convection heat transfer from a sphere at low Prandtl numbers," *Int. J. Thermal Sci.*, vol. 184, Feb. 2023, Art. no. 107970.

[7] J. W. Kim, S.-B. Woo, J. I. Song, and H.-K. Kwon, "An observational study of hydrodynamic impact on water mass transport due to tidal power generation," *Sci. Total Environ.*, vol. 807, Feb. 2022, Art. no. 151013.

[8] C.-H. Hui, C.-F. Lo, and H.-Y. Ip, "Modelling asymmetric unemployment dynamics: The logarithmic-harmonic potential approach," *Entropy*, vol. 24, no. 3, p. 400, Mar. 2022.

[9] S. Simonyan and S. Bayraktar, "Asymmetric dynamics in sovereign credit default swaps pricing: Evidence from emerging countries," *Int. J. Emerg. Markets*, Mar. 2022, doi: 10.1108/IJOEM-03-2021-0469.

[10] X. Cheng, J. Fei, X. Li, X. Huang, and W. Yang, "The research progress in secondary eyewall formation and eyewall replacement cycle of typhoon," *Acta Geophys. Sinica*, vol. 64, no. 6, pp. 1857–1868, Jun. 2021.

[11] T. Liu, Q.-G. Wang, and H.-P. Huang, "A tutorial review on process identification from step or relay feedback test," *J. Process Control*, vol. 23, no. 10, pp. 1597–1623, Nov. 2013.

[12] O. Miguel-Escrig, J.-A. Romero-Pérez, J. Sánchez-Moreno, and S. Dormido, "Multiple frequency response points identification through single asymmetric relay feedback experiment," *Automatica*, vol. 147, Jan. 2023, Art. no. 110749.
[13] R. J. Kochenburger, "Analyzing contactor servomechanisms by frequency-response methods," *Electr. Eng.*, vol. 69, no. 8, pp. 687–692, Aug. 1950.
[14] K. J. Åström and T. Hägglund, "Automatic tuning of simple regulators with specifications on phase and amplitude margins," *Automatica*, vol. 20, no. 5, pp. 645–651, Sep. 1984.
[15] S.-K. Kim and C. K. Ahn, "Auto-tuner-based controller for quadcopter attitude tracking applications," *IEEE Trans. Circuits Syst. II, Exp. Briefs*, vol. 66, no. 12, pp. 2012–2016, Dec. 2019.
[16] A. Gelb and W. E. Van der Velde, *Multiple-input Describing Functions and Nonlinear System Design*. New York, NY, USA: McGraw-Hill, 1968.
[17] P. Wang, D. Gu, and W. Zhang, "Modified relay feedback identification based on describing function analysis," *Ind. Eng. Chem. Res.*, vol. 46, no. 5, pp. 1538–1546, Feb. 2007.
[18] J. Lee, S. W. Sung, F. Y. Lee, M. Baldea, and T. F. Edgar, "Full closed-loop tests for the relay feedback autotuning of stable, integrating, and unstable processes," *ACS Omega*, vol. 4, no. 20, pp. 18760–18770, Oct. 2019.
[19] D. Simhachalam, S. Talukder, R. K. Mudi, and C. Dey, "Enhanced critical point assessment with relay feedback," *Mech. Syst. Control*, vol. 46, no. 4, pp. 170–180, Dec. 2018.
[20] S. Pandey and S. Majhi, "System identification under relay and PI control," *IEEE Trans. Circuits Syst. II, Exp. Briefs*, vol. 67, no. 6, pp. 1089–1093, Jun. 2020.
[21] S.-H. Shen, H.-D. Yu, and C.-C. Yu, "Use of saturation-relay feedback for autotune identification," *Chem. Eng. Sci.*, vol. 51, no. 8, pp. 1187–1198, Apr. 1996.
[22] Q.-G. Wang, T. H. Lee, and L. Chong, *Relay Feedback: Analysis, Identification and Control*. London, U.K.: Springer, 2012.
[23] K. K. Tan, T. H. Lee, S. Huang, K. Y. Chua, and R. Ferdous, "Improved critical point estimation using a preload relay," *J. Process Control*, vol. 16, no. 5, pp. 445–455, Jun. 2006.
[24] C. H. Jeon, Y. J. Cheon, J.-S. Kim, J. Lee, and S. W. Sung, "Relay feedback methods combining sub-relays to reduce harmonics," *J. Process Control*, vol. 20, no. 2, pp. 228–234, Feb. 2010.
[25] P. Ghorai, S. Majhi, V. R. Kasi, and S. Pandey, "Parameter identification of delayed under-damped systems using on-line relay autotuning," *IEEE Trans. Circuits Syst. II, Exp. Briefs*, vol. 66, no. 7, pp. 1197–1201, Jul. 2019.
[26] I. Kaya and D. P. Atherton, "Parameter estimation from relay autotuning with asymmetric limit cycle data," *J. Process Control*, vol. 11, no. 4, pp. 429–439, Aug. 2001.
[27] B. E. Park, K. H. Kim, H. S. Kang, S. W. Sung, and I.-B. Lee, "Improved relay feedback method under noisy and disturbance environments," *J. Chem. Eng. Jpn.*, vol. 52, no. 5, pp. 430–438, May 2019.
[28] B. S. Taysom and C. D. Sorensen, "Adaptive relay autotuning under static and non-static disturbances with application to friction stir welding," *ISA Trans.*, vol. 97, pp. 474–484, Feb. 2020.
[29] Q.-G. Wang, C.-C. Hang, and Q. Bi, "A technique for frequency response identification from relay feedback," *IEEE Trans. Control Syst. Technol.*, vol. 7, no. 1, pp. 122–128, Jan. 1999.
[30] M.-D. Ma and X.-J. Zhu, "A simple auto-tuner in frequency domain," *Comput. Chem. Eng.*, vol. 30, no. 4, pp. 581–586, Feb. 2006.
[31] M. Hofreiter, "Fitting anisochronic models by method of moments for anisochronic control of time delay systems," *Int. J. Math. Models Methods Appl. Sci.*, vol. 10, no. 1, pp. 71–79, Jan. 2016.
[32] J. S. Moreno, S. D. Bencomo, O. M. Escrig, and J. A. R. Pérez, "Asymmetric delayed relay feedback identification based on the *n*-shifting approach," *Int. J. Control*, Aug. 2021, doi: 10.1080/00207179.2021.1962968.
[33] K. V. Ramana, S. Majhi, and A. K. Gogoi, "Modeling and estimation of DC–DC buck converter dynamics using relay feedback output with performance evaluation," *IEEE Trans. Circuits Syst. II, Exp. Briefs*, vol. 66, no. 3, pp. 427–431, Mar. 2019.
[34] M. Hofreiter, "Shifting method for relay feedback identification," *IFAC-PapersOnLine*, vol. 49, no. 12, pp. 1933–1938, Jan. 2016.
[35] J. S. Moreno, S. D. Bencomo, and J. M. D. Martínez, "Fitting of generic process models by an asymmetric short relay feedback experiment—The n-shifting method," *Appl. Sci.*, vol. 11, no. 4, Feb. 2021, Art. no. 1651.
[36] Q. Bi, Q.-G. Wang, and C.-C. Hang, "Relay-based estimation of multiple points on process frequency response," *Automatica*, vol. 33, no. 9, pp. 1753–1757, Sep. 1997.
[37] T. Liu, F. Gao, and Y. Wang, "A systematic approach for on-line identification of second-order process model from relay feedback test," *AIChE J.*, vol. 54, no. 6, pp. 1560–1578, Jun. 2008.
[38] S. Pandey, S. Majhi, and P. Ghorai, "A new modelling and identification scheme for time-delay systems with experimental investigation: A relay feedback approach," *Int. J. Syst. Sci.*, vol. 48, no. 9, pp. 1932–1940, Feb. 2017.
[39] K. H. Kim, J. E. Bae, S. C. Chu, and S. W. Sung, "Improved continuous-cycling method for PID autotuning," *Processes*, vol. 9, no. 3, Mar. 2021, Art. no. 509.
[40] M. T. D. Silva and P. R. Barros, "A robust relay feedback structure for processes under disturbances: Analysis and applications," *J. Control, Autom. Electr. Syst.*, vol. 30, no. 6, pp. 850–863, Aug. 2019.
[41] S. W. Sung and J. Lee, "Relay feedback method under large static disturbances," *Automatica*, vol. 42, no. 2, pp. 353–356, Feb. 2006.
[42] M. R. Spiegel, *Theory and Problems of Laplace Transforms* (Schaums Outline Series). New York, NY, USA: McGraw-Hill, 1965.
[43] Q.-G. Wang, T. H. Lee, and K. K. Tan, *Finite-Spectrum Assignment for Time-Delay Systems*. London, U.K.: Springer, 1999.
[44] L. Pekař, M. Song, S. Padhee, P. Dostálek, and F. Zezulka, "Parameter identification of a delayed infinite-dimensional heat-exchanger process based on relay feedback and root loci analysis," *Sci. Rep.*, vol. 12, no. 1, Jun. 2022, Art. no. 9290.
[45] K. J. Aström and T. Hägglund, *Advanced PID Control*, 2nd ed. Research Triangle Park, NC, USA: The Instrumentation, Systems, and Automation Society, 2006.
[46] J. A. Nelder and R. Mead, "A simplex method for function minimization," *Comput. J.*, vol. 7, no. 4, pp. 308–313, Jan. 1965.
[47] H. Guzowski, M. Smolka, A. Byrski, L. Pekar, Z. K. Oplatkova, R. Senkerik, R. Matusu, and F. Gazdos, "Effective parametric optimization of heating-cooling process with optimum near the domain border," in *Proc. IEEE 11th Int. Conf. Intell. Syst. (IS)*, Warsaw, Poland, Oct. 2022, pp. 1–6, doi: 10.1109/IS57118.2022.10019630.

LIBOR PEKAŘ (Member, IEEE) was born in Zlín, Czech Republic, in 1979. He received the B.S. degree in automation and informatics, the M.S. degree in automation and control engineering in consumption industry, and the Ph.D. degree in technical cybernetics from Tomas Bata University (TBU) in Zlín, in 2002, 2005, and 2013, respectively. He was an Associate Professor of machine and process control with TBU in Zlín, in 2018. From 2006 to 2013, he was a Junior Lecturer with TBU in Zlín, where he became a Senior Lecturer, in 2013. Since 2020, he has been a Senior Lecturer with the College of Polytechnics Jihlava, Czech Republic. He is the author of one book and eight book chapters and the (co)author of more than 50 journal articles and 75 conference papers. His research interests include analysis, modeling, identification, and control of time-delay systems, algebraic control methods, heat-exchanger processes, auto tuning, and optimization techniques.

He received the Laureate of the ASR Seminary Instrumentation and Control, in 2007 and 2009; the Rectors' Award for the Best Ph.D. Thesis at the Faculty of Applied Informatics, TBU in Zlín, in 2013; the Best Reviewer Award from *Control Theory and Technology* journal, in 2019; and the Outstanding Paper Award at the first World Conference on Multiphase Transportation, Conversion, and Utilization of Energy, in 2022. He has served as a Reviewer for over 30 scientific journals, including *Automatica*, IEEE TRANSACTIONS ON AUTOMATIC CONTROL, IEEE TRANSACTIONS ON INDUSTRIAL ELECTRONICS, IEEE CONTROL SYSTEMS LETTERS, IEEE ACCESS, and *ISA Transactions*. He serves as an Academic Editor for *Mathematical Problems in Engineering*, a Topical Advisory Panel Member and a Lead Guest Editor for *Mathematics*, an Editorial Board Member for *AppliedMath*, an Advisory Board Member for *Applied Thermal Engineering*, and an Associate Editor for *International Journal of Robotics and Control Systems*.

RADEK MATUŠŮ (Member, IEEE) was born in Zlín, Czech Republic, in 1978. He received the M.S. degree in automation and control technology in consumer goods industry from the Faculty of Technology, Tomas Bata University (TBU) in Zlín, in 2002, and the Ph.D. degree in technical cybernetics from the Faculty of Applied Informatics (FAI), TBU in Zlín, in 2007.

He was appointed an Associate Professor of machine and process control at FAI, TBU in Zlín, in 2018. He has been holding various research or pedagogical positions at TBU in Zlín, since 2004, where he is currently a Researcher and a Project Manager. He has (co) authored more than 50 scientific journal papers and over 110 conference contributions. His research interests include analysis and synthesis of robust control systems, fractional-order systems, and algebraic methods in control design.

Prof. Matušů is a member of Topical Advisory Panel of *Mathematics* and *Fractal and Fractional*. He has also served as a Reviewer for over 50 scientific journals, including *Automatica*, IEEE TRANSACTIONS ON AUTOMATIC CONTROL, and *IEEE Control Systems Magazine*. He serves as an Academic Editor for *Journal of Control Science and Engineering*. He was a Guest Editor of *Mathematic Problems in Engineering*.

MENGJIE SONG was born in Hebei, China, in 1984. He graduated from Hunan University, Harbin Institute of Technology, and The Hong Kong Polytechnic University, in 2008, 2010, and 2015, respectively.

He worked as Research Fellow, JSPS Research Fellow, and DECRA Research Fellow in the Nanyang Technological University, University of Tokyo and University of Wollongong, respectively. He was appointed as a Professor of complicated phase change thermal fluid and built the Frost Laboratory at the Department of Energy and Power Engineering, School of Mechanical Engineering, Beijing Institute of Technology in 2019. He was selected into the National Youth Talent Project in 2021. He is a Guest Professor of Tomas Bata University in Zlín, Czech Republic.He focuses on the mechanism study of heat and mass transfer coupled with the flow for nearly 15 years. On the topics of frosting, icing, boiling, phase change, he proposed a series of definitions to describe thermophysical phenomena, such as even/uneven frosting/defrosting, and frosting/defrosting evenness value. Currently, he has published 155 journal articles, in which 123 ones are SCI, with 84 ones as first/corresponding author, and 8 ones were ESI.

Prof. Song is the Editor-in-Chief of *Recent Patents on Mechanical Engineering* (EI, Scopus) and an Associate Editor of *Frontiers in Energy Research* (SCI). From 2020 to 2022, he was selected into the World's Top 2% Scientists list (Singleyr).

LENKA KUKLIŠOVÁ PAVELKOVÁ received the M.S. degree in engineering cybernetics from the Faculty of Electrical Engineering, Czech Technical University (CTU), in 1992, and the Ph.D. degree in engineering informatics from the Faculty of Transportation, CTU, in 2009. From 2001 to 2009, she was with the Department of Adaptive Systems, Institute of Information Theory and Automation (IITA), Czech Academy of Sciences (CAS), as a Research Assistant, where she has been a Research Associate, since 2009. Since 2017, she has been a Lecturer with the College of Polytechnics Jihlava, Czech Republic.

QINGBIN GAO received the B.S. degree in mechanical engineering from the Harbin Institute of Technology, China, in 2011, and the Ph.D. degree in mechanical engineering from the University of Connecticut, in 2015. He was an Assistant Professor with the Department of Mechanical and Aerospace Engineering, California State University, Long Beach, from 2015 to 2018. In 2019, he joined the School of Mechanical Engineering and Automation, Harbin Institute of Technology (Shenzhen), as an Associate Professor. His main research focuses on the stability analysis and control synthesis of time-delay systems, with applications to multi-agent systems, vibration control, and robotics.

He was a recipient of the Best Conference Paper Award of the 19th International Conference on Networking, Sensing, and Control (ICNSC), in 2017; and the sixth American Society of Mechanical Engineers (ASME) Dynamic Systems and Control Conference (DSCC), in 2013. He is currently an Associate Editor of IEEE TRANSACTIONS ON INTELLIGENT TRANSPORTATION SYSTEMS, *Artificial Intelligence Review*, and *International Journal of Adaptive Control and Signal Processing*.